

2016

Co-axial biopen printing for articular cartilage regeneration

Malachy Kevin Maher
mkm290@uowmail.edu.au

Follow this and additional works at: <https://ro.uow.edu.au/theses>

University of Wollongong

Copyright Warning

You may print or download ONE copy of this document for the purpose of your own research or study. The University does not authorise you to copy, communicate or otherwise make available electronically to any other person any copyright material contained on this site.

You are reminded of the following: This work is copyright. Apart from any use permitted under the Copyright Act 1968, no part of this work may be reproduced by any process, nor may any other exclusive right be exercised, without the permission of the author. Copyright owners are entitled to take legal action against persons who infringe their copyright. A reproduction of material that is protected by copyright may be a copyright infringement. A court may impose penalties and award damages in relation to offences and infringements relating to copyright material.

Higher penalties may apply, and higher damages may be awarded, for offences and infringements involving the conversion of material into digital or electronic form.

Unless otherwise indicated, the views expressed in this thesis are those of the author and do not necessarily represent the views of the University of Wollongong.

Recommended Citation

Maher, Malachy Kevin, Co-axial biopen printing for articular cartilage regeneration, Master of Philosophy thesis, Australian Institute of Innovative Materials, University of Wollongong, 2016. <https://ro.uow.edu.au/theses/4942>

Research Online is the open access institutional repository for the University of Wollongong. For further information contact the UOW Library: research-pubs@uow.edu.au



**UNIVERSITY
OF WOLLONGONG
AUSTRALIA**

Co-axial biopen printing for articular cartilage regeneration

**Malachy Kevin Maher
BSc (Biomedical Science)**

This thesis is presented as part of the requirements for the award

Master of Philosophy (M.Phil)
from
The University of Wollongong

September 2016

Intelligent Polymer Research Institute (IPRI)

Australian Institute of Innovative Materials (AIIM)

The University of Wollongong

Certification

I, Malachy Kevin Maher, declare that this dissertation, submitted in conjunction with the required coursework fulfills the requirements for awarding the degree of Master of Philosophy, within the AIIM Faculty at the Intelligent Polymer Research Institute, University of Wollongong. All work is my own unless referenced, acknowledged or stated otherwise. This document has not been submitted for qualifications at any other academic institution.

Acknowledgements

I would like to thank my supervisors Dr Zhilian Yue and Prof Gordon Wallace for their expertise and guidance throughout the project. From weekly meetings to help in the laboratory, this work is a direct reflection of their knowledge and passion for extending scientific knowledge.

Special thanks to the clinical mentors Professor Peter Choong and Dr Claudia Di Bella, for their clinical perspective and specialist knowledge of the requirements of the end product.

I would like to extend my thanks for the assistance provided to me by the diverse team at The Australian Institute for Innovative Materials (AIIM), and specifically The Intelligent Polymer Research Institute (IPRI) throughout the entirety of the project. Specifically Dr Hai Xin, the additive manufacturing team; Dr Stephen Beirne, Fletcher Thompson, Dr Cormac Fay, Adam Taylor, Ali Jeiranikhameneh and Chris Richards, for their expertise, ingenuity and friendliness. Fellow Masters students Ariel Cherny, Jeremy Di Noro and Charles Hamilton as well as PhD students who provided advice, Rob Murphy, Sepehr Talebian, Rodrigo Lozano and Cody Wright.

Abstract

The co-axial Biopen printing tool offers promise to house cells and regenerate articular cartilage. The use of gelatin methacrylamide (GelMA) in combination with hyaluronic acid methacrylate (HAMA) has been a favorable combination for extrusion printing and potential cell growth.

GelMA and HAMA were synthesized and formulated as a bi-component ink. The potential of the ink for co-axial printing was examined. In particular, the viscoelastic properties of the ink were investigated in order to establish optimal printing conditions. Favorable printing properties were demonstrated in the ink with both shear-thinning and rapid self-recovery characteristics. Lithium phenyl-2,4,6-trimethylbenzoylphosphinate (LAP) was selected as the photo-initiator for crosslinking of the bioink at 400 nm. The effect of light attenuation in the ink was investigated by UV spectroscopy, and the ink crosslinking kinetics were examined at 400 nm using *in situ* rheology.

The physical properties of the photo-crosslinked gel as a shell component for co-axial extrusion printing were investigated as a function of LAP concentration and light intensities. The gels were able to hold more than 90 wt% water with Young's Moduli up to 150 kPa, depending on the degree of crosslinking. The diffusion of molecules through the GelMA/HAMA hydrogel were measured using a custom designed, 3D printed diffusion chamber. The glucose diffusion coefficient of the gel was similar to those in alginate and gelatin hydrogels used in similar studies.

Finally, printing with the co-axial Biopen system was successful with consistent lines printable at various extrusion rates and core: shell ratios.

Table of Contents

Certification.....	3
Acknowledgements.....	4
Abstract.....	5
List of Figures.....	8
List of Tables	12
1 Introduction.....	13
1.1 Osteoarthritis.....	13
1.2 The basic science of articular cartilage.....	13
1.2.1 Composition of articular cartilage.....	14
1.2.2 Articular cartilage zones.....	18
1.2.3 Development.....	19
1.3 Current treatment	19
1.4 Cartilage tissue engineering	20
1.4.1 Hydrogels	20
1.4.2 Photo-initiated crosslinking.....	21
1.4.3 Hydrogels in cartilage tissue engineering.....	22
1.4.4 Cell source.....	26
1.5 Bioprinting.....	27
1.6 Biopen.....	30
1.7 Aims.....	33
2 Materials and Methods.....	34
2.1 Material synthesis	34
2.2 NMR Characterization	34
2.3 Ink formulation and characterization	35
2.4 Photo-crosslinking kinetics of GelMA/HAMA by LAP.....	37
2.4.1 Light attenuation study.....	37
2.4.2 <i>In-situ</i> UV cross-linking rheology.....	38
2.5 Physicochemical characterization of GelMA/HAMA hydrogels.....	38
2.5.1 Sample Preparation	38
2.5.2 Free polymer loss.....	39
2.5.3 Equilibrium water uptake.....	39
2.5.4 Mechanical properties of the cross-linked GelMA/HAMA hydrogels	39
2.5.5 Diffusion.....	40
2.6 Co-axial printing.....	42
3 Results and discussion	44
3.1 Material functionalization and characterization.....	44
3.2 Ink characterization	46
3.3 Photo-induced crosslinking kinetics of ink	53
3.3.1 Light attenuation.....	53
3.3.2 Crosslinking kinetics	55
3.4. Physicochemical characterization of the photo-cross-linked GelMA/HAMA hydrogel as shell component	58

3.4.1 Free polymer loss.....	58
3.4.2 Equilibrium water content	59
3.4.3 Gel mechanical properties	59
3.4.4 Diffusion characteristics	61
3.5. Co-axial printing.....	63
4.0 Conclusions.....	69
Appendix	70
References	73

List of Figures

Figure 1. Schematic illustration of the structure of aggregates in healthy articular cartilage. A) Hyaluronic acid is the backbone of the compound, with branching aggrecan molecules. These aggrecan molecules have side chains of GAGs, which attract water. B) The aggregates can be seen amongst collagen fibers. The surrounding free space will be filled primarily with fluid drawn in by the highly polar side chains (GAGs).

Figure 2. Zones of articular cartilage, demonstrating the collagen fiber arrangement and chondrocyte shapes.

Figure 3. The Biopen developed at the Intelligent Polymer Research Institute (IPRI), The University of Wollongong. The nozzles show the entry ports for the two cartridges and their junction as they form the core-shell structure.

Figure 4. Diffusion chamber. A) Render of the custom designed diffusion chamber, designed in Solidworks with Adam Taylor and printed on the Connex inkjet printer. B) Chamber assembled. C) Cross-section of chamber where the hydrogel sample is loaded. D) Example of a gradient created between the two chambers with fluorescence.

Figure 5. Biopen attached to XY-plotter in order to control the rate of movement and gap distance to substrate.

Figure 6. Schematics of (A) methacrylation of gelatin to form gelatin methacrylamide (GelMA), and (B) methacrylation of Hyaluronic acid to form Hyaluronic acid Methacrylamide (HAMA). (C) LAP-initiated photo-crosslinking process of GelMA/HAMA.

Figure 7. ^1H -NMR spectra for Gelatin, and GelMA. The green region represents the phenylalanine signal (6.9 – 7.5 ppm), and grey region represents the lysine group

(2.8 – 2.95 ppm).

Figure 8. Rheological temperature scans from 5°C to 40°C at 2°C/min at a fixed shear of 0.01s^{-1} . A) Shows the 10% GelMA sample dissolved in PBS. B) The 2% HAMA sample dissolved in PBS and C) The GelMA/HAMA (10%/2%) samples dissolved in PBS. The gelation point of GelMA was seen to be at $\sim 10^\circ\text{C}$, which increased in the GelMA/HAMA sample to $\sim 17^\circ\text{C}$. A general increase in the sample modulus of GelMA/HAMA was seen at all points compared to GelMA. The modulus of the HAMA sample was seen to be largely independent of temperature.

Figure 9. Rheological oscillation scans of GelMA/HAMA at 5°C. A) Strain sweep from 1-100% strain, (frequency fixed at 1 Hz) with a large linear visco-elastic region up until $\sim 20\%$. B) Frequency scan from 1-100 Hz (Strain fixed at 1%).

Figure 10. Rheology scans performed with GelMA/HAMA at 5°C. A) Depicts the shear-thinning effect seen during the shear rate scan, with the viscosity decreasing as the shear rate increases. B) The step strain graph using a low strain of 1% and a high strain of 100% to disrupt the internal network of the GelMA/HAMA. C) Shows a close up of the recovery of the ink in B after the high strain is released. D) Shows the yield point of GelMA/HAMA ($\sim 900\text{ Pa}$).

Figure 11. A and B) UV-vis absorbance at 400nm of LAP dissolved in PBS and LAP in GelMA/HAMA. C) 400 nm UV light penetration depth in PBS and GelMA/HAMA with 0.12% LAP, calculated by using the Beer-lambert equation with the UV-vis data. D) Penetration depth of 400 nm UV light in GelMA/HAMA with 0.06 wt% and 0.12 wt% LAP.

Figure 12. Cross-linking kinetics of GelMA/HAMA (10%/2% dissolved in PBS). Two different concentrations of LAP were used (0.06 and 0.12 wt%) and three different levels of irradiation energy were applied (144, 288 and 408 mJ). A 60 second calibration period was allowed before the light was applied for 60 seconds, and a 60 second post exposure period is also shown.

Figure 13. Modulus of GelMA/HAMA samples immediately after UV-crosslinking at 400 nm. Various concentrations of the LAP photo-initiator were used (0.06 and 0.12 wt%) as well as three levels of irradiation energy applied (144, 288 and 408 mJ).

Figure 14. Free polymer loss of the photo-crosslinked GelMA/HAMA hydrogels. Two concentrations of the LAP photo-initiator were used (0.06 and 0.12 wt%) as well as three levels of irradiation energy applied (144, 288 and 408 mJ).

Figure 15. Equilibrium water content of the photo-crosslinked GelMA/HAMA hydrogels. Two concentrations of the LAP photo-initiator were used (0.06 and 0.12 wt%) as well as three levels of irradiation energy applied (144, 288 and 408 mJ).

Figure 16. Young's Modulus of the photo-crosslinked GelMA/HAMA hydrogels. Samples were created with 0.06 wt% and 0.12 wt% LAP and treated with three levels of irradiation energy (144, 288 and 408 mJ).

Figure 17. Glucose diffusion through the photo-crosslinked GelMA/HAMA hydrogels (disk = 15 mm diameter, 1.5mm thick).

Figure 18. A) Biopen extrusion rates ($\mu\text{L}/\text{min}$) at varying core:shell ratios and the total extrusion settings 5, 10 and 15. B) Biopen extrusion rates at a 50:50 core:shell ratio, and the total extrusion settings 5, 10 and 15. The equation of the line is included so that exact volumetric extrusion rates ($\mu\text{L}/\text{min}$) can be calculated at any extrusion setting.

Figure 19. Microscopic images of extruded Biopen lines at a flow setting of 8 (0.25 mL/min) and 12 (0.36 mL/min), pen movement speed of 7.5 mm/s and a gap distance of 0.25 mm.

Figure 20. Strut width of the Biopen extruded lines measured from microscopic images. Strut width was seen to increase as the overall extrusion rate increased, but also as a high proportion of core was extruded. Lines printed at a 50:50 core-shell ratio at the extrusion setting of 8 (0.25 mL/min) were significantly thinner than lines printed at the high extrusion rate of 12 (0.36 mL/min) at core-shell ratios of

25:75 and 10:90 ($p < 0.05$). Inset is the cross-section of a co-axially extruded line, with the core-shell division visible. Printed at flow setting of '8' (0.25 mL/min) and a core:shell ratio of 50:50.

Figure 21. Temperature rheology scans with the addition of nano-hydroxyapatite. A control was used with no added hydroxyapatite and while three different amounts of hydroxyapatite were measured (0.5, 1.0 and 2.0 wt%).

Figure 22. Young's Modulus of GelMA/HAMA samples with added nano-hydroxyapatite (0, 0.5, 1.0 and 2.0 wt%).

List of Tables

Table 1. Components of articular cartilage and their relative composition

Table 2. Location and function of the five types of collagen found in articular cartilage.

Table 3. Summary of the main additive manufacturing techniques currently used.

Table 4. Summary of conditions used in ^1H - NMR. The Bruker AVANCE III 600 NMR was used for experimentation.

Table 5. Summary of the parameters used for the dynamic oscillation time, frequency and amplitude scans of GelMA/HAHA ink.

Table 6. Rate of UV-crosslinking with the LAP photo-initiator and 400nm light. Two different photo-initiator concentrations were used (0.06 and 0.12 wt%) and three levels of light exposure (144, 288 and 408 mJ).

Table 7. Summary of the glucose diffusion experiments performed in triplicate, showing the lag time and diffusion co-efficient of glucose determined for each experiment.

Table 8. Biopen extrusion rates at various extrusion settings and core: shell ratios. Water was used and weighed (assuming 1mL = 1g). The core:shell ratio was varied from 0% core to 100% core, and three extrusion settings were used.

1 Introduction

1.1 Osteoarthritis

Osteoarthritis (OA) is a common, disabling condition affecting nearly 9% of the Australian population and is becoming an increasingly expensive health challenge for the community (Donaldson, Tudor, & McDermott, 2015). Osteoarthritis is a chronic degenerative joint disease that leads to inflammation and degradation of articular cartilage. This results in bone rubbing against bone causing joint stiffness, swelling and pain (Ryan, 2015). The initiation and progression of OA involves mechanical, structural, genetic and environmental factors (March & Bagga, 2004). The prevalence of OA increases with age, with more than 50% of people aged above 65 suffer from the condition and by 85 years the condition is universally present (Saffarian, Mohammadi, & Mohammadi, 2015). This ubiquitous condition is the second highest cause of disability in America (after cardiovascular disease) and translates to an annual cost to Australian healthcare of AUD\$3.7 billion (Bruyère et al., 2015). Any measures that can prevent the progression of the disease or the need for expensive surgical joint replacements are important and vital health interventions.

The purpose of this project is to utilize a gelatin-hyaluronic acid based hydrogel for co-axial biopen printing. By examining the characteristics of the hydrogel we can further improve the ink properties for cell therapy using co-axial Biopen printing. The ultimate goal is to deliver tissue-engineering solutions for cartilage repair and regeneration.

1.2 The basic science of articular cartilage

There are three types of cartilage; hyaline cartilage, elastic cartilage and fibrocartilage. Hyaline cartilage is the most abundant type found on many joint surfaces. Elastic cartilage is found in the larynx and outer ear, and has a similar composition to articular cartilage, but with more elastic fibers (Ye et al., 2013). Fibrocartilage is the only type of cartilage that contains both type 1 and type 2

collagen, and is found at the pubis symphysis, the annulus fibrosis of intervertebral disks and is present at the bone-tendon interface (Ye et al., 2013).

Articular cartilage is hyaline cartilage on diarthrodial joint surfaces, including the knee, hip and shoulder (P. J. Roughley & Lee, 1994). In the knee specifically, it is found on the superior articular surface of the tibia, the inferior articular surface of the femur and the posterior surface of the patella (Flanigan, Harris, Brockmeier, Lathrop, & Siston, 2014). This articular cartilage is characterized by high levels of proteoglycans, and is responsible for low friction articulation and shock absorption (Di Bella, Fosang, Donati, Wallace, & Choong, 2015). The tissue is avascular and aneural meaning it has limited capacity for self-healing, a notion which underlies the imperativeness of the preservation and health of the tissue.

1.2.1 Composition of articular cartilage

Articular cartilage is comprised of five main components including fluid, collagen, proteoglycans, chondrocytes and glycoproteins and their relative compositions are listed in Table 1. Chondrocytes are the major cell type in cartilage and originate as mesenchymal stem cells (MSC). The MSCs differentiate into chondroblasts, which aggregate and form chondrocytes. The chondrocytes produce and maintain the cartilaginous matrix, which predominantly consists of collagen and proteoglycans.

Proteoglycans are proteins that are found in connective tissue and account for 10-15% of the wet weight of articular cartilage (Sophia Fox, Bedi, & Rodeo, 2009). The function of each proteoglycan is determined by their protein core and glycosaminoglycan (GAG) side chains. The largest and most prevalent proteoglycan is aggrecan, which consists of many chondroitin sulphate and keratin sulphate chains. Aggrecan is highly polar and hence attracts water, which results in the characteristic low friction and high compressive strength seen in articular cartilage. Aggrecan interacts with hyaluronic acid (HA) and link protein (LP) to form large proteoglycan aggregates. These large proteoglycan aggregates are comprised of a

central HA chain, with up to 100 aggrecan molecules branches (Sophia Fox, Bedi, & Rodeo, 2009). This high-density polar structure seen in Figure 1 draws a large amount of water in. High aggrecan content, high glycosaminoglycan substitution and large aggregate chains are typical in healthy articular cartilage. Damaged articular cartilage results in impaired aggrecan function, due to either proteolytic cleavage of the protein core from the side chains (resulting in decreased fluid retention) or cleavage of HA which decreases aggregate size (P.J Roughley, 2006). The other proteoglycans found in articular cartilage are collectively called small leucine rich repeat proteoglycans (SLRP) which maintain tissue integrity and assist with metabolism (P.J Roughley, 2006).

Table 1. Components of articular cartilage and their relative composition

Component	% Total weight
Chondrocytes	1-5%
Fluid	65-80%
Collagen	10-20% wet weight (60% dry)
Proteoglycan	10-15% wet weight
Glycoproteins and lipids	<2% wet weight

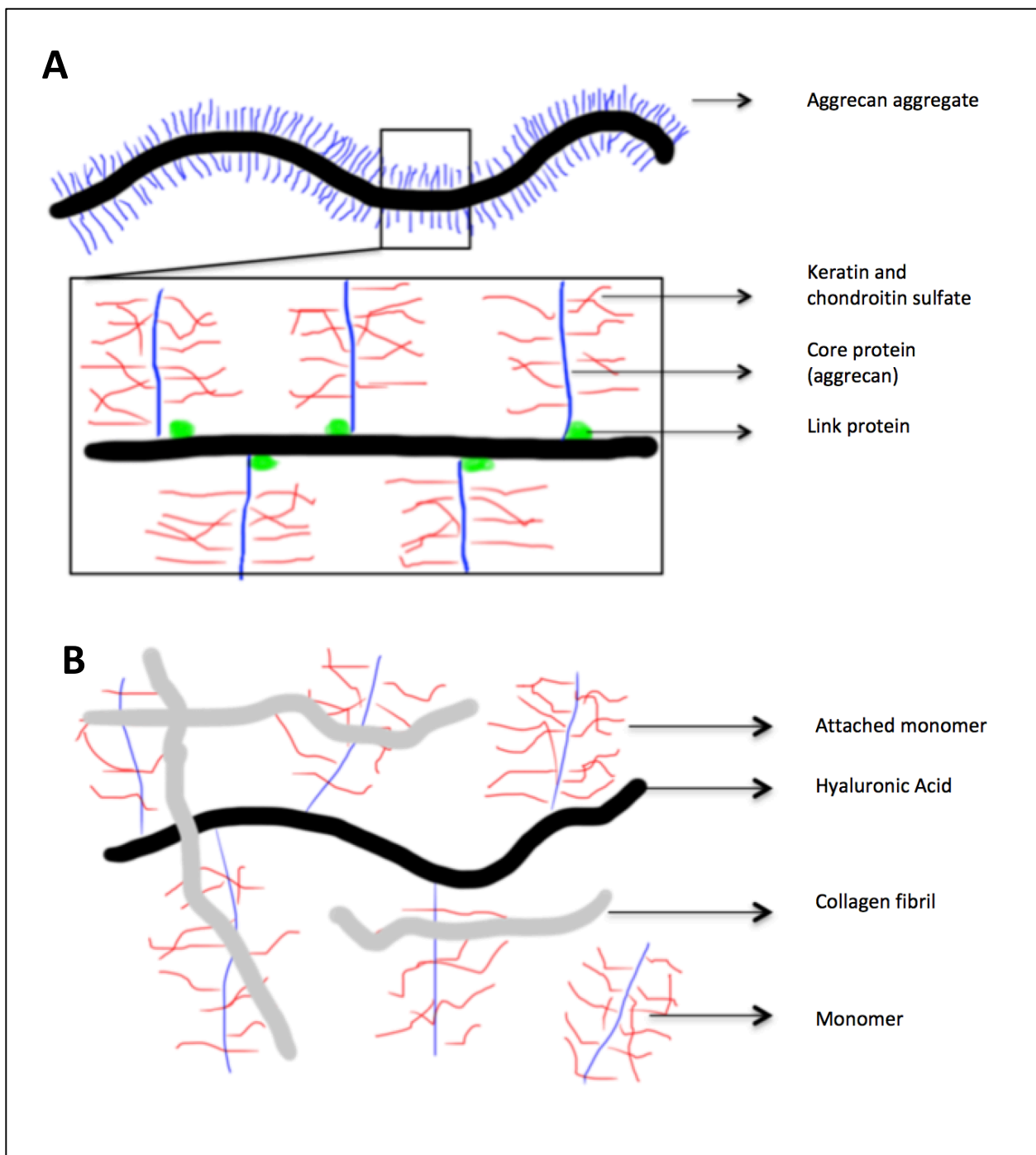


Figure 1. Schematic illustration of the structure of aggregates in healthy articular cartilage. A) Hyaluronic acid (~10 μm long) is the backbone of the compound and has aggrecan molecule branches. These aggrecan molecules have side chains of GAGs, which attract water. B) The aggregates can be seen amongst collagen fibers. The surrounding free space will be filled primarily with fluid drawn in by the highly polar side chains (GAGs).

Collagen is the structural framework of cartilage and accounts for 60% of the dry weight (10-20% wet weight). Collagen is a protein that is composed of a triple helix. While 28 types of collagen exist, only five types are present in articular cartilage, as shown in Table 2 (Flanigan et al., 2014). Collagen type 2 is most abundant in articular cartilage, accounting for up to 95% of all the collagen present. The remaining collagen is type VI, IX, X and XI, all of which have roles in producing and stabilizing the type 2 collagen. Collagen is formed when the amino acids glycine and proline (amongst others) form a three-dimensional structure, called procollagen. This procollagen then undergoes modification as hydroxyl groups are added to the proline and lysine groups. The type of collagen that is created depends on the location and how many hydroxyl groups are added. The process of cartilage formation is termed chondrogenesis. During chondrogenesis, type 2 procollagen genes are activated (COL2A1, type 2A and type 2B) which work to promote collagen type 2 formation (Panadero, Lanceros-Mendez, & Ribelles, 2016).

Table 2. The location and function of the five types of collagen found in articular cartilage.

Collagen type	Location	Function
Type II	Articular Cartilage	Strength
Type VI	Chondron basket microfilaments	Helps chondrocytes attach to matrix
Type IX	Fibril-associated collagen	Tensile properties and inter-fibrillar connections
Type X	Hypertrophic chondrocyte in calcified cartilage layer	Structural support and aids in cartilage mineralization
Type XI	Fibril template	Nucleates fibril formation

1.2.2 Articular cartilage zones

Articular cartilage can be divided into three regions as illustrated in Figure 2. Firstly, the superficial zone (tangential) orientates its collagen fibers parallel to the joint to provide shear strength. Here the chondrocytes are flattened, collagen fibers condensed, there are few proteoglycans and is the only region of articular cartilage where progenitor cells have been identified (Paunipagar & Rasalkar, 2014). The smooth surface in this layer is important for low friction, smooth articulation in the joint. Secondly, the intermediate zone houses collagen type 2 fibers in an oblique or random orientation. This zone is the thickest, has round chondrocytes and is responsible for majority of the compressive strength seen in cartilage. The final layer is the deep layer (basal layer) where the type 2 collagen fibers are perpendicular to the joint surface. This region is responsible for adhesion and has round chondrocytes arranged in columns and the highest concentration of proteoglycans. Deeper to the basal layer is the tidemark, which separates the superficial un-calcified articular cartilage from the deeper calcified cartilage. The calcified cartilage is on the surface of the subchondral bone. These regions act together to provide the compressive strength and low friction articulation characteristic of articular cartilage.

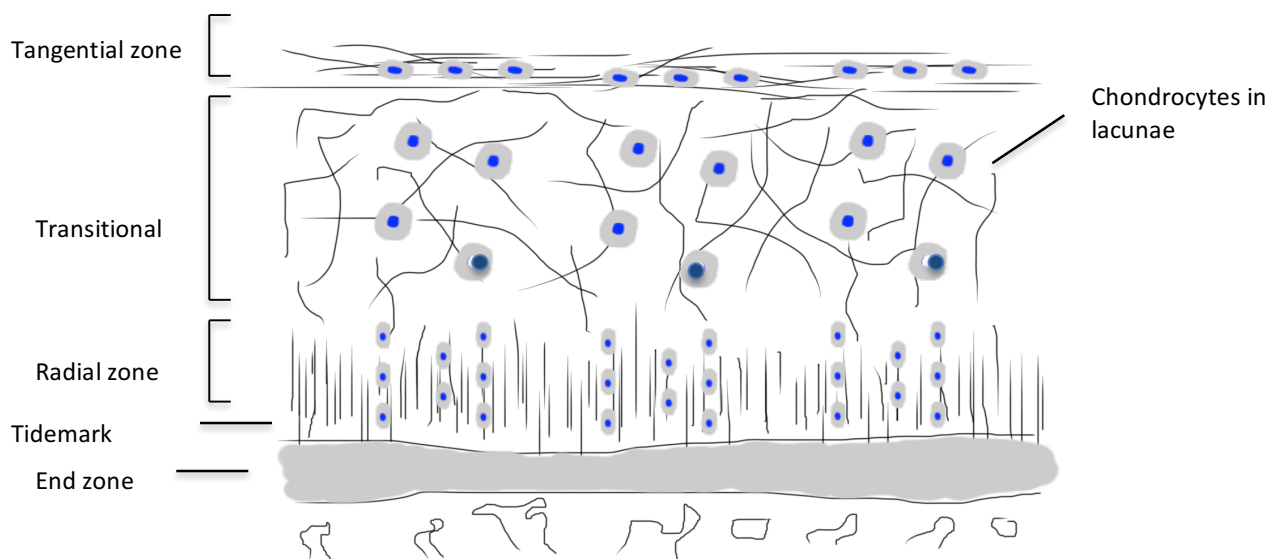


Figure 2. Zones of articular cartilage, showing the collagen fiber arrangement and chondrocyte shapes.

1.2.3 Development

Chondrogenesis is the process of cartilage formation and occurs when mesenchymal stem cells condense and chondroprogenitor cells undergo differentiation (Fox et al., 2009). Following chondrogenesis, the chondrocytes can follow one of two pathways. Firstly, they can remain as resting cells to form the articular cartilage or undergo proliferation and terminal differentiation to form hypertrophic chondrocytes. These cells will later undergo endochondral ossification, where they are replaced by bone.

1.3 Current treatment

Currently the treatment for osteoarthritis in the knee is palliative and focused after the cartilage and underlying bone is damaged. Losing weight and correcting posture and walking technique are early measures that can reduce the rate of damage, however surgical intervention is frequently required. The most basic procedure involves injecting corticosteroids or hyaluronic acid into the knee to reduce inflammation and allow for smoother articulation. However, further surgical intervention is required. An arthroscopy involves a surgeon using minimally invasive keyhole surgery to clean the surface of the joint. This can be used in early cases or in young individuals. Microfractures are another procedure that is used and involves drilling small holes into the bone, where fibrocartilage (scar tissue) will later form (Falah et al., 2010). This technique is used as it stops the bone on bone rubbing, however, still isn't ideal as fibrocartilage is scar tissue and does not mimic the smooth native articular cartilage. While 95% of patients report satisfaction with the procedure, complications do occur and patients can be immobilized for long periods of time. Mosaicplasty is a technique that is also used which involves harvesting autologous osteochondral tissue from less-load bearing regions and transplanting them to defected areas. If the degradation of cartilage and bone continues to persist, invasive and expensive partial and total knee replacements may be required.

1.4 Cartilage tissue engineering

Cartilage is avascular and aneural, meaning that it does not directly receive any blood or nerve innervation. Because of this, we cannot feel damage to our articular cartilage and the body's ability to self-repair damaged cartilage is low. Early on, researchers tried to inject chondrocytes and mesenchymal stem cells into damaged regions in the hope to regenerate cartilage (Huang, Hu, & Athanasiou, 2016). It was soon realized that these cells needed support and nutrients to grow, and so began the quest to find a suitable material to house and grow these cells. Early work identified that there were four main principles critical to cartilage tissue engineering; the cells, growth factors, scaffold material and the mechanical environment they are exposed to (Kessler & Grande, 2008). Growth factors such as BMP-6 and TGF- β_2 have been shown to help direct MSC's towards chondrogenesis, as well as hyaluronic acid, a natural glycosaminoglycan found abundantly in healthy joints (Muzzarelli, Greco, Busilacchi, Sollazzo, & Gigante, 2012). The two main cells used in cartilage tissue engineering are chondrocytes and mesenchymal stem cells. Both offer distinct advantages and disadvantages that will be discussed later. Over the years, different combinations of hydrogels, cells and growth factors have been investigated in an effort to optimize cartilage tissue engineering.

1.4.1 Hydrogels

Hydrogels are highly hydrated polymer networks that consist of natural or synthetic polymers. Typical examples of hydrogels include, but not limited to, poly(ethylene glycol) (PEG), poly(vinyl alcohol), alginate, chitosan, collagen and gelatin based systems (Karunanithi et al., 2016). They have been used widely as materials in contact lenses, drug delivery and as scaffolds in tissue engineering (Sivashanmugam, Arun Kumar, Vishnu Priya, Nair, & Jayakumar, 2015). In tissue engineering, hydrogels create a favorable environment with structural and mechanical properties often mimicking soft tissue. The intended function of these hydrogels when used as a scaffold is to deliver seeded cells into the desired location in the

body, encourage cell adhesion, growth and differentiation, allow for diffusion of nutrient molecules and provide suitable mechanical support.

As scaffolding materials, hydrogels are generally characterized by a number of properties, such as biocompatibility, degradation, mechanical properties, molecule diffusion and swelling properties. It is important to understand the correlation between hydrogel structures and these properties. Parameters of hydrogel structures include polymer composition, molecular weight and concentration, and type and degree of crosslinking. Varying any of these parameters can alter the scaffolds properties and the way that it performs (Kessler & Grande, 2008). For example, by using a higher molecular weight polymer it often creates a stronger scaffold due to the increased molecule entanglement (Kessler & Grande, 2008).

Most hydrogels are derived from water soluble polymers, which necessitates a crosslinking mechanism in order to render the structure stable within a timeframe as specified by a given application (Ju, Kim, & Lee, 2001). Depending on polymer structure, physical crosslinking can be induced by electrostatic complexation, hydrogen bonding or hydrophobic interactions (Billiet, Vandenhaute, Schelfhout, Van Vlierberghe, & Dubruel, 2012). Chemical crosslinking occurs when permanent covalent bonds are created, which can be achieved via various mechanisms, e.g. enzymatic, redox-mediated, functional group reactions and free-radical photopolymerisation (Brownsey, 1993). Hydrogels can also prepared be a combination of both chemical and physical means (El-Sherbiny & Yacoub, 2013).

1.4.2 Photo-initiated crosslinking

Among the above crosslinking methods, photo-initiated crosslinking has been most extensively explored in 3D printing. Taking gelatin and hyaluronic acid as an example, by modifying the polymers with methacryloyl moieties, rapid crosslinking can be achieved in a controlled manner, using either ultraviolet (UV) or visible light (VIS) depending on the type of photo-initiators. (Klotz, Gawlitta, Rosenberg, Malda, & Melchels, 2016). This rapid crosslinking is favorable for extrusion based printing to achieve high resolution structures.

The most commonly used photo-initiator is 1-[4-(2-hydroxyethoxy)-phenyl]-2-hydroxy-2-methyl-1-propane-1-one, also known as Irgacure 2959. This initiator has limited water solubility and produces a benzoyl and ketyl-free radical upon UV exposure at 365 nm (Liu, Li, Xue, & Phillips, 2014). Most cell encapsulation studies that utilize this initiator report low cytotoxicity, however exposing cells to UV-light can be detrimental to DNA and protein function. Many researchers agree that subtle damage could occur that would not be identified without long term studies (Klotz, Gawlitta, Rosenberg, Malda, & Melchels, 2016). For this reason, photo-initiators which are excited by light in the less damaging visible range (390-700nm) would be looked to for promise. A recently synthesized photo-initiator that is excited in this range is lithium phenyl-2,4,6-trimethylbenzoylphosphinate (LAP). This water-soluble initiator is less studied but has shown promising cell viability and gelation results in polyethylene glycol diacrylate (PEGDA) (Henrikson et al.; Huber, Borchers, Tovar, & Kluger, 2016; Lin, 2014). Aside from being excited at the safer wavelength of 400-405 nm, LAP has been shown to induce gelation of PEGDA 10 times faster than Irgacure 2959, when both were exposed to 365 nm light (Fairbanks, Schwartz, Bowman, & Anseth, 2009). This instantaneous cross-linking is favorable as extruded lines can be rapidly cross-linked without losing their shape. LAP does however have a narrow excitation peak, between 400-405 nm, and becomes less efficient at longer wavelengths.

1.4.3 Hydrogels in cartilage tissue engineering

Many natural and synthetic polymers have been used to fabricate scaffolds for cartilage tissue engineering. Research has sought to find the best combination of material, scaffold design, cells and growth factors that can be used in cartilage tissue engineering.

Alginate is a polysaccharide derived from brown seaweed. Alginate hydrogels remain one of the most explored natural hydrogels in a wide range of tissue engineering applications, including cartilage. Studies have shown that alginate

based hydrogels support cartilage formation and can achieve similar mechanical properties as native cartilage (Lima et al., 2006). In a clinical trial by *Selmi et al.* 2008, 17 patients with chondral defects received alginate based scaffolds with suspended chondrocytes. Their mean International Knee Documentation Committee (IKDC) scoring system improved from a preoperative score of 37/100, to 77.8/100 after 2 years (Selmi et al., 2008).

Chitosan is a polysaccharide derived from exoskeleton of crustaceans. It is a low cost, biocompatible material with antibacterial properties and a structure similar to GAGs (Yuan et al., 2015). Chondrocytes have been encapsulated into chitosan scaffolds and have successfully repaired non-weight bearing cartilage defects, and integrated well with surrounding tissue (Hao et al., 2010). However, chitosan is not water soluble at neutral pH, so acetic acid is often used to facilitate the polymer dissolution or chemical modifications are made to the chitosan (Croisier & Jérôme, 2013). The other main drawback of chitosan is its low stability when used *in situ*. These can be improved through chemical modification of chitosan, facilitating its application in cartilage tissue engineering.

PEG is a very common synthetic polymer used in cartilage tissue engineering. Synthetic polymers are favourable for use as they are reliably produced and modifiable, creating mechanically strong constructs (Bryant, Bender, Durand, & Anseth, 2004; Kloxin, Kasko, Salinas, & Anseth, 2009). Chondrocytes and MSCs have been encapsulated into PEG based hydrogels and in the presence of growth factors, cartilage has formed (Elisseff et al., 1999; Sharma, Williams, Khan, Manson, & Elisseff, 2007). PEG does have limited bioactivity, and requires chemical modification with cell adhesion motif and/or addition of growth factors to promote cell adhesion, migration, proliferation and differentiation.

Gelatin is a natural polymer formed by hydrolysis of collagen extracted from the skin, bone and connective tissue of animals. This proteinaceous substance is comprised of denatured and partially hydrolyzed native collagen, mainly type 1 (Young, Wong, Tabata, & Mikos, 2005). Gelatin retains important bioactive

sequences from collagen, e.g. arginine-glycine-aspartic acid peptide, which are required for integrin-mediated cell attachment (Vandooren, Van den Steen, & Opendakker, 2013). This integrin-mediated cell adhesion allows essential cellular functions such as migration, proliferation and differentiation to occur (Heino, Huhtala, Kapyla, & Johnson, 2009; Nichol et al., 2010). As gelatin remains soluble at body temperature, it needs to be cross-linked to offer adequate mechanical support. By modifying gelatin with methacrylic anhydride we can form gelatin-methacrylamide (GelMA), a material that can be crosslinked when exposed to light. The degree of modification, as well as the intensity and duration of photo-initiated crosslinking alters the properties of the GelMA, which consequently changes the mechanical and diffusion properties of the scaffold. Although the articular cartilage's ECM is complex, GelMA mimics the ECM closely and because of its inherent cell adhesion sites and matrix metalloproteinase response peptide motifs which allows cells to easily proliferate and migrate. GelMA has been used widely in bone, cartilage, vascular and cardiac tissues engineering amongst others. *Schuurman et al.* 2013 found that GelMA hydrogels have modifiable mechanical and swelling properties depending on the polymer concentration and amount of UV irradiation delivered. *Visser et al.* 2015 investigated the effect of the addition of tissue-derived matrices to GelMA hydrogels with chondrocytes and MSCs. While the addition of tissue-derived matrices to GelMA affected chondrogenic differentiation of MSCs, no subsequent improvement was noted. For chondrocytes, the addition of the tissue-derived matrices impaired their function in GelMA (*Visser et al.*, 2015).

Hyaluronic acid (HA) is the most common natural non-sulfated glycosaminoglycan found in connective tissue coating chondrocytes and synovial fluid. It increases the viscosity of synovial fluid and enhances chondrogenesis by assisting mesenchymal condensation by binding on the cell surface receptor CD44 (*Akmal et al.*, 2005; *Chung & Burdick*, 2009; *Liao, Yaszemski, Krebsbach, & Hollister*, 2007). Studies from *Levett et al.* 2014 demonstrated that the combination of hyaluronic acid with GelMA produced a promising cell environment and mechanical strength. The scaffolds underwent a 3-fold increase in their compressive modulus after 8 weeks cultivation

and the encapsulated chondrocytes displayed the favorable rounded morphology (Levett, Hutmacher, Malda, & Klein, 2014). *Chang et al.* 2013 combined HA with poly(lactide-co-glycolide) (PLGA) and found improvements in the mechanical properties of the scaffold as well as cell attachment, proliferation and extracellular matrix production (N.-J. Chang, Jhung, Yao, & Yeh, 2013).

Composite hydrogels have been developed by the combination of multiple polymers to achieve improved physical and/or biological properties. *Karunanithi et al.* 2016 found that the combination of alginate and fucoidan, a natural polysaccharide, improved chondrogenesis in MSC's (Karunanithi et al., 2016). *Kundu et al.* 2015 combined the synthetic polycaprolactone with the natural alginate and found improved chondrogenesis after 4 weeks while *Chang et al.* 2013 combined the natural chitosan with nano-hydroxyapatite and saw improved mechanical properties in the scaffold (C. Chang et al., 2013; Kundu, Shim, Jang, Kim, & Cho, 2015). These composite materials offer promise for tissue engineering as they can incorporate favorable properties of two or more polymers.

1.4.4 Cell source

Researchers have sought to investigate the most suitable cell types to promote chondrogenesis. The two main candidates are cartilage's native cells, chondrocytes and the earlier stage mesenchymal stem cells. *Levatt et al.* found some success growing chondrocytes as confirmed by increased COL2A1 and ACAN gene expression and increased production of ECM (collagen type 2 and aggrecan) (P. A. Levett et al., 2014). Harvesting chondrocytes for use for implantation is difficult, compared to extracting MSCs. Chondrocytes only constitute 2-5% of cartilage, and as such, they require expansion prior to use. Expansion can cause dedifferentiation of mature chondrocytes, a decrease in production of proteoglycans and collagen type 2 (necessary for articular cartilage formation), alongside an increase in the production of the less desirable type 1 collagen.

Adipose tissue is a rich, readily available and minimally invasive source of MSCs (Mueller et al., 2010). MSCs are multipotent stromal cells that can differentiate into osteoblasts (bone cells), chondrocytes (cartilage cells), myocytes (muscle cells) and adipocytes (fat cells). Through different combinations of growth factors and environments, the MSCs can be directed towards one specific cell type. Most commonly TGF- β_2 and BMP-6 are added to the MSC's in pellet culture which directs the proliferating chondrocytes to express Sox9 and collagen type II, with further differentiate to form hypertrophic chondrocytes (Mueller et al., 2010). Myers and his group have completed a series of experiments on the ability of human intra-patella fat pad (hIPFP) derived MSCs to be directed towards cartilage formation (Felimban et al., 2014). They utilized pellet culture and determined by gene analysis that the hIPFP MSCs could be directed towards cartilage formation. After this, in collaboration with the Intelligent Polymer Research Institute (IPRI), they used a 3D printed natural polysaccharide chitosan scaffold to house the cells. This showed similar rates of chondrogenesis, as the chitosan is porous and allows for diffusion and cell growth. The quest for optimizing the extracellular environment for chondrogenesis of hIPFP has then led to the recent study using a bi-component scaffold based on modified gelatin and hyaluronic acid. Both gelatin and hyaluronic

acid were modified with methacrylic anhydride to prime the molecules for UV initiated cross-linking. Hyaluronic acid (HA) was added to enhance chondrogenesis as it has been shown to play a critical role in mesenchymal condensation through binding on the CD44 receptor (Bian et al., 2013). Additionally, HA further increases the viscosity of the hydrogel precursor and thus the printability.

1.5 Bioprinting

Additive manufacturing is the production of three-dimensional models through layer-by-layer construction. In early years, processes such as milling and injection molds were most common but with advances in technology, 3D printing has evolved. 3D printing differs from traditional manufacturing, as it is an additive process, depositing material layer-by-layer rather than a reductive process like milling. 3D printing also allows us to create gradients (mechanical strength, pore size, concentration of cells ect) within a printed structure, allowing for different properties where they are needed most. This is ideal for prototyping and medical purpose.

The three main methods of 3D bioprinting include inkjet, micro-extrusion and laser assisted deposition. Each of these three modalities has been used in tissue engineering and their key features are highlighted in table 3.

3D inkjet bioprinters were originally developed from commercially made 2D inkjet printers (Tao Xu, Kincaid, Atala, & Yoo, 2008). Modern 3D inkjet printers are optimized to print biological materials at high resolution and speed, using either thermal or acoustic forces to extrude droplets. Thermal inkjet printers heat the print head up to 300°C to produce jettable droplets. Studies has shown that such printing process does not significantly affect the viability of printed cells (T. Xu, Jin, Gregory, Hickman, & Boland, 2005). While these thermal inkjet printers are widely available, low cost and fast, there is concern with these printers as they can expose cells to mechanical stresses, have variable droplet sizes and unreliable cell encapsulation (Tao Xu, Atala, & Yoo, 2008). The other main type of inkjet printer utilizes a piezoelectric nozzle, creating acoustic waves in the material to extrude the droplets.

This method produces uniform droplet size and does not expose the cells to heat and pressure stresses.

For inkjet printing, ink materials must meet very constrained physical limits for viscosity and surface tension (T. Xu et al., 2005). In the case of cell printing, this translates to a low cell density ($<10^6$ cells/ml, (Murphy & Atala, 2014)) and a low concentration polymer ink. These pose a significant challenge for inkjet printing, if not combining with other printing approaches, to deliver tissue constructs of clinically-relevant sizes and with biologically-relevant cell densities.

Micro extrusion printers are the most common biological printer and utilize a 3-axis stage fitted with an automatically extruding pneumatic or mechanical syringe to print lines. More advanced micro extruders have multiple ink cartridges, temperature control for thermo-sensitive hydrogels, a UV light source inbuilt to facilitate photo-crosslinking after extrusion and a video camera for imaging and quality control. Materials which exhibit a flow property called shear thinning are often used in micro extrusion. Shear thinning is a phenomenon whereby the viscosity of a material decreases as a shear is applied. As the material is extruded from the nozzle (shear force applied), the viscosity drops which subsequently causes the stress on the material within the nozzle to drop, creating a favorable environment for cells. After the material leaves the nozzle and the shear force is removed, the viscosity can recover and the extruded material can form high-resolution structures. Micro-extrusion allows use of very high cell density inks (R. Chang, Nam, & Sun, 2008; Smith et al., 2004), and is a popular biofabrication tool for producing clinically relevant tissues.

Laser assisted bioprinting is a less common approach that uses a laser to selectively cure droplets of a photo-curable material in a vat. As this approach does not have a nozzle it is free from clogging, can use materials with a wide range of viscosity's and high cell concentrations up to 10^8 cells/mL, but remains an expensive and slow technique (Murphy & Atala, 2014).

Table 3. Summary of the main bioprinting techniques (Malda et al., 2013; Mandrycky, Wang, Kim, & Kim, 2016; Murphy & Atala, 2014)

Bioprinting modality	Inkjet	Micro-extrusion	Laser assisted bioprinting
Material viscosity	Narrow (3.5-12 mPa/s)	Wide, 30 mPa/s to $>6 \times 10^7$ mPa/s	1-300 mPa/s
Print speed	Fast (1-10,000 drops/second)	Slow (10-50 $\mu\text{m/s}$)	Fast (200-1,600 mm/s)
Resolution	50 μm	5 – 50 μm	10 μm
Cell viability	>85%	40-86%	>95%
Cell density	Low, $<10^6$ cells/mL	High	Medium, 10^8 cells/mL
Printer cost	Low	Medium	High

1.6 Biopen

Following on from principles developed in commercial extrusion printers, a handheld surgical tool called the Biopen was developed towards *in-situ* cell therapy in an operating room. As surgeons do not know the size or severity of articular cartilage defects before they operate, a simple handheld device that can be used in the operating room is ideal.

The Biopen was developed as a co-axial extrusion device in a collaboration between the Intelligent Polymer Research Institute (IRPI) at The University of Wollongong, and with surgeons at The University of Melbourne and St Vincent's Hospital, Melbourne. The co-axial morphology is favorable for bioprinting, as it allows for a low density core where we can house cells, and the shell can be crosslinked with LAP and 405 nm light, providing mechanical support. Many iterations of the handheld device have been developed, but the current version has 60 mechanical components, 21 electrical components and uses a mechanical extrusion mechanism, with built in fiber optic fibers to allow for UV initiated crosslinking at the nozzle tip. The core component has a diameter of 400 μm , a wall thickness of 200 μm separating the core and shell, and the shell component has a diameter of 800 μm (minus the 600 μm core).

For instance, *O'Connell et al. 2016* used the Biopen for co-axial extrusion of GelMA/HAMA. This work used an early version Biopen that used pneumatic pressure for extrusion and the Irgacure 2959 photo initiator. It was seen that there was 70% transmittance of the 365 nm UV -A light at 1 mm, the ink had inherent properties suitable to printing including shear-thinning and there was >97% cell viability after 1 week (O'Connell et al., 2016).

More recent versions of the Biopen have switched to a mechanical extrusion system. The pen maintains the two 'ink' cartridges, which extrude through a co-axial nozzle to form a core-shell product, as seen in Figure 3. It is envisaged that the core would be used for cell growth while the shell will provide the mechanical support for the cells. As the core and shell can be extruded at different rates, the thicknesses of each

component can be varied in response to the required properties, such as mechanical strength and diffusion of molecules. This customizable system allows for easy tailoring of the scaffold properties for each patient.

The Biopen was created with significant input from Orthopedic surgeon Peter Choong, regarding the intended use. The IPRI team completed the fabrication and testing (ongoing).

Gordon Wallace	Head of institute
Stephen Beirne	Head of additive fabrication, IPRI
Peter Choong	Orthopedic surgeon involved in the ideation of the Biopen
Fletcher Thompson	Engineer
Cathal O'Connell	PhD student who worked on the Biopen

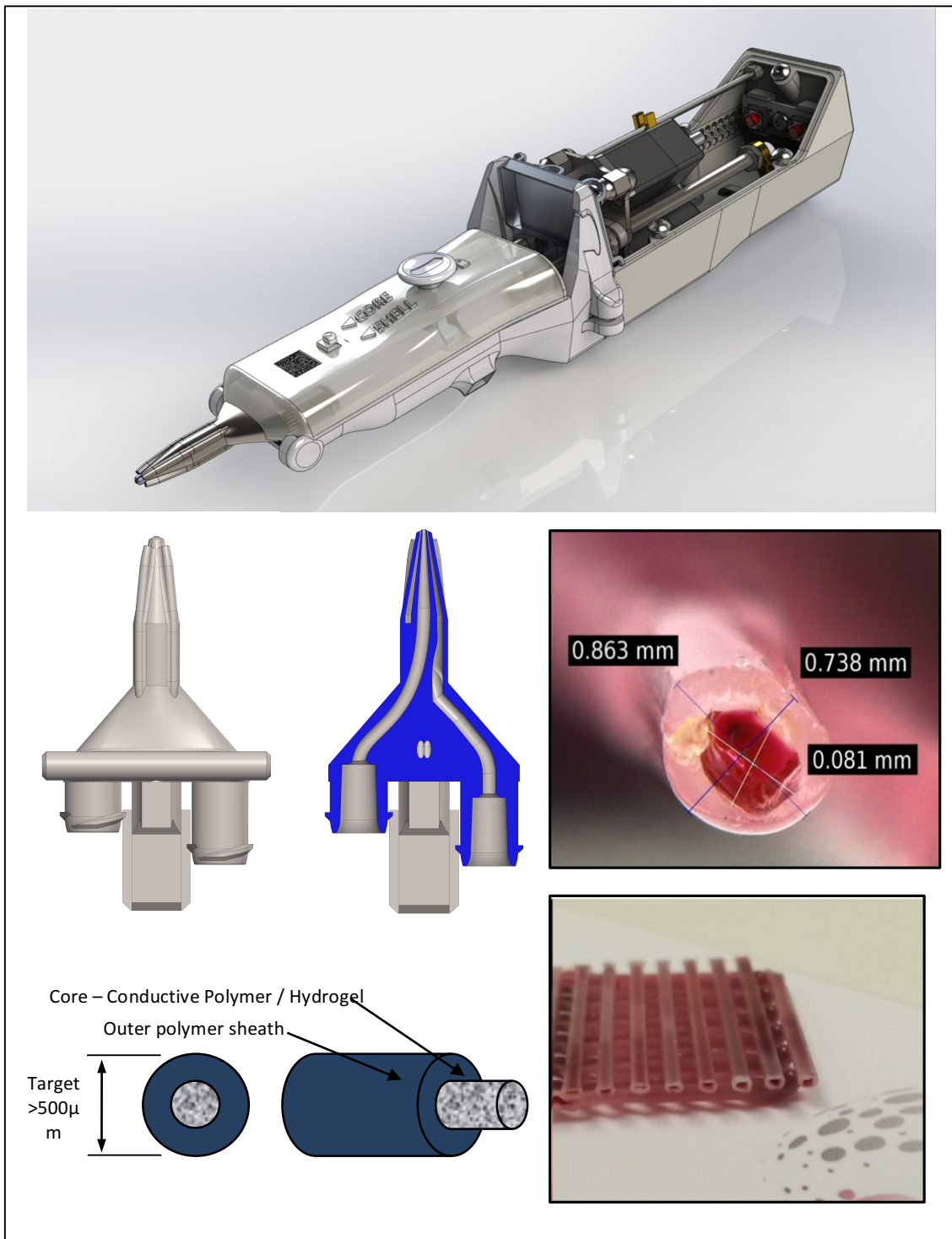


Figure 3. The Biopen developed at the Intelligent Polymer Research Institute (IPRI), The University of Wollongong. The nozzles show the entry ports for the two cartridges and their junction as they form the core - shell structure.

1.7 Aims

This project involves the use of a custom-designed handheld co-axial printing tool called the Biopen for the fabrication of cell-laden constructs for cartilage repair and regeneration. The constructs will be fabricated from methacrylate-functionalized gelatin (GelMA) and Hyaluronic acid (HAMA) that will be photo-cross-linked upon extrusion. The overall aim of the project is to understand the suitability of the material for extrusion printing from the existing Biopen for articular cartilage regeneration. The specific aims of this project are to:

1. Synthesize ink materials including GelMA and HAMA
2. Examine the visco-elasticity and printability of ink
3. Investigate the photo-induced crosslinking kinetics of ink
4. Investigate the physiochemical properties of the photo-crosslinked hydrogel as shell component
5. Perform co-axial Biopen printing

2 Materials and Methods

2.1 Material synthesis

The composite GelMA-HAMA material was made by synthesizing both the GelMA and the HAMA components then mixing them. The methacrylation of gelatin and hyaluronic acid was performed to allow for photo-crosslinking later. 20 g of Gelatin powder (Type A, 300 bloom, Sigma Aldrich) was dissolved in 200 mL of phosphate buffered saline (PBS) at 50°C then autoclaved. All work was completed in a laminar flow hood that was sterilized with UV light for 20 minutes and each piece of equipment was wiped with 70% ethanol to minimize contamination. While the gelatin solution was being stirred at 50°C, 16 mL of methacrylic anhydride (MA) was added drop wise and the reaction allowed to continue for 3 hours. In order to terminate the methacrylation, 600 mL of PBS was then added. 5 mL of chloroform was added to the above solution, which was then thoroughly dialyzed against deionized water at 40°C for 7 days. The product was then collected by freeze-drying and stored at -20°C. This entire reaction yielded 20 g of GelMA.

To synthesize the HAMA component, 1 g of sodium hyaluronate (HA, Pharma Grade 150, 1200-1900 kDa) was dissolved in 200 mL of sterilized water. 7 mL of MA (20 times excess) was added to the solution. The reagent amount was calculated relative to a total of four hydroxyl groups per HA disaccharide unit. The pH of the reaction mixture was maintained at 8.5 by adding 5M NaOH. After the pH was stable, the reaction was stirred overnight. Again, 1.5 mL of chloroform was added to the solution to minimize contamination. The resulting solution was dialyzed against deionized water (12- 14 MWCO) for 48 hours and freeze dried then stored at -20°C. This reaction yielded 1 g of HA-MA.

2.2 NMR Characterization

¹H-NMR was used to determine the degree of methacrylation of GelMA. 5 mg of gelatin and GelMA were dissolved in 0.6 mL of deuterated water (D₂O) respectively

and transferred into NMR tubes. The Bruker AVANCE III 600 machine was used and Bruker Topspin 3.2 and IconNMR software was used to analyse the data. Table 4 summarizes the experimental protocol.

Table 4. Summary of conditions used in ^1H NMR. The Bruker AVANCE III 600 NMR was used for experimentation.

Number of scans	128
Temperature	40°C
Spectral width (Frequency)	6400 Hz
Acquisition time	2.6 s
Impulse	308
Transients	208

2.3 Ink formulation and characterization

The freeze dried GelMA and HAMA were dissolved together in sterile phosphate buffered saline (PBS) to achieve a concentration of 10% GelMA and 2% HAMA. To facilitate the dissolution, the mixture was vortexed regularly and placed in a 37°C water bath for 72 hours or until transparent. This sample was wrapped in aluminum foil and stored at -20°C.

In order to investigate how the GelMA/HAMA ink behaves while being extruded from the Biopen, rotational and oscillatory rheological measurements were undertaken using a TA instruments AR-G2 rheometer, fitted with a 40 mm, 2° Peltier cone plate. The ink samples were removed from the freezer (-20°C) and placed in a 37°C water bath for 30 minutes prior to experimentation.

For each rheological experiment, 0.6 mL of the GelMA/HAMA sample was loaded onto the Peltier stage. At a gap distance of 500 microns, a pre-shear of 5 s^{-1} was applied to all samples for 5 minutes to eliminate memory in the gel. After the initial temperature scan, all tests were performed at 5°C. Between each experiment, the stage was cleaned and a fresh sample loaded.

The first set of tests performed was an oscillatory temperature sweep. The temperature of the plate was ramped from 40°C to 5°C at a rate of 2°C/min, while a constant shear rate of 0.01 s^{-1} was applied. The storage moduli (G') and viscous moduli (G'') were recorded over the range. Then other oscillatory rheological measurements were performed, including time, amplitude and frequency sweep. The test parameters are listed in Table 5. The initial time sweep was performed for 30 minutes, at a fixed frequency of 1 Hz and strain of 1% to ensure that the material was stable at these low forces. This time sweep ensures that any change seen in subsequent frequency and strain sweeps is only a result of the variable, rather than the ink degrading over time. By performing the strain sweep, we can determine the Linear Visco-elastic Region (LVR), which is the level of strain which the sample can withstand before it begins to break down. During the frequency sweep the % strain is kept constant. The constant % strain used in the frequency sweep needs to be within this linear region, to ensure that any change seen in the sample modulus is solely due to the change in frequency (variable).

Shear viscosity measurement were conducted in a rotational mode with shear rate ranging from 0.001 s^{-1} to 1000 s^{-1} over a 20 minute period.

Step-strain oscillatory measurements were performed to investigate the recovery of the ink and to mimic the extrusion printing process. The ink was maintained at 0.1 % strain for 2 minutes then an abrupt increase in strain to 100 % was held for 3 minutes, which was repeated 3 times. The samples modulus was recorded over this range.

Table 5. Summary of the parameters used for the oscillatory rheological measurement, including time, amplitude, and frequency sweep of GelMA/HAMA ink.

Experiment type	Constant	Variable	Measure
Time Oscillation	Frequency = 1 Hz Strain = 1%	Time (30 minutes)	Modulus (Pa)
Amplitude Oscillation (Strain sweep)	Frequency = 1 Hz	Strain = 0.1 – 100%	Modulus (Pa)
Frequency Oscillation	Strain = 1%	Frequency = 1 – 100 Hz	Modulus (Pa)

2.4 Photo-crosslinking kinetics of GelMA/HAMA by LAP

2.4.1 Light attenuation study

UV-vis spectroscopy was employed to study the light attenuation effect in photo crosslinking of GelMA/HAMA. Various concentrations of the LAP photo-initiator were dissolved into PBS and also GelMA/HAMA, respectively. The GelMA/HAMA samples were centrifuged to remove air bubbles. The molar absorptivity of LAP in PBS and GelMA/HAMA were determined by plotting the sample absorbance measured at 400 nm as a function of LAP concentration, using the Beer-Lambert law as shown below,

$$A = \epsilon cl \quad \text{Equation 1}$$

Where A represents absorbance; ϵ is the molar absorptivity of the photo-initiator ($L \text{ mol}^{-1} \text{ cm}^{-1}$ at 400 nm); l is the path length (depth of penetration); and c is the concentration of photo-initiator (mol/L).

Using the molar absorptivity obtained, percent transmittance was calculated as a function of light penetration depth, using the Beer-Lambert law shown below:

$$T = 10^{(2-A)} = 10^{(2-\epsilon cl)} \quad \text{Equation 2}$$

2.4.2 In-situ UV cross-linking rheology

Using the Physicia MCR 301 rheometer, fitted with a 12 mm flat plate and the 400 nm UV-light source used previously, the storage moduli of the GelMA/HAMA samples were measured during the course of photo-crosslinking. Samples of GelMA/HAMA at various concentrations of photo-initiator (0.06 and 0.12 wt%) were used to determine the effect of the photo-initiator on crosslinking strength. At the same 5 cm gap distance, the UV-light source was set-up to provide three energy outputs (144 mJ, 288 mJ and 408 mJ) for photo-crosslinking.

Using a 15 mm flat plate, the rheometer was set at a constant 4°C, 1 Hz and 10% strain. The GelMA/HAMA was loaded and recording started. A 60 second period was given to see the baseline modulus, then the 400 nm light was turned on for 60 seconds, after which another 60 second monitoring period was given.

2.5 Physiochemical characterization of GelMA/HAMA hydrogels

2.5.1 Sample Preparation

GelMA/HAMA samples were prepared with a dimension of 15 mm diameter and 1.5 mm height, using a customized sample mold. Using the ULS PLS5MW laser cutter, 1.5 mm thick sheets of Perspex were cut to produce squares (20×20 mm). Within these squares, a circle of 15 mm diameter was cut from the middle. These pieces were then placed on a glass slide. GelMA/HAMA was dissolved in PBS. The LAP photo-initiator was then added to the GelMA/HAMA at different concentrations (0.06 and 0.12 wt%). These samples were centrifuged to remove small air bubbles.

The gel was then placed into the wells, and a cover slip was placed on top, creating a sandwich with a solid disk of GelMA/HAMA inside. The whole slide was then exposed to the 400 nm light at different intensities, for 60 seconds, at a 5 cm gap distance, which equal to an irradiation energy level of 144, 288 and 408 mJ, respectively. After crosslinking, the Perspex was removed from the slide and the disk of GelMA/HAMA was easily removed.

2.5.2 Free polymer loss

The as-prepared samples of GelMA/HAMA were freeze dried and weighed. After this they were washed with PBS for 5 days, changing the PBS twice daily. Then the samples were again freeze dried and weighed. The decrease in mass was calculated, and was related to the amount of un-crosslinked polymers.

2.5.3 Equilibrium water uptake

After removal of the free polymer, the samples were washed with water and freeze dried. They were rehydrated and the equilibrium water uptake was determined by measuring the increase in mass.

2.5.4 Mechanical properties of the cross-linked GelMA/HAMA hydrogels

The photo-crosslinked hydrogels were also subject to mechanical testing. Using the Texas Instruments EZ-S, a 10N sensor was attached and calibrated. The head of the instrument was cylindrical and 1 mm in diameter. An indentation depth of 0.15 mm (10% of the disk thickness) was used and the resistance recorded as the probe indented for 10 seconds.

Methods established from *Naficy et al.* 2013 were used to calculate the value of Young's Modulus. Firstly the reduced modulus (E^*) was calculated from equation 3.

$$F = 2aE^*d \quad \text{Equation 3}$$

$$(E^*)^{-1} = (1 - V_1^2)E_1^{-1} + (1 - V_2^2)E_2^{-1} \quad \text{Equation 4}$$

where;

F = applied force (N)

d = indentation depth (mm)

a = indenter radius (0.5mm)

E₁ and E₂ = Indenter substrate moduli

V₁ and V₂ = Poisson's Ratio

Poisson's ratio accounts for the deformation in the sample during compression. For visco-elastic polymers, a Poisson's Ratio of 0.5 is often used. Assuming that the indenter is infinitely rigid, Equations 3 and 4 can be simplified to find Young's Modulus (McKee, Last, Russell, & Murphy, 2011):

$$F = \left(\frac{8}{3}\right) aE_2d \quad \text{Equation 5}$$

2.5.5 Diffusion

A customized diffusion chamber was designed using Solidworks and 3D printed on the Objet Connex 500-inkjet printer. The diffusion chamber is comprised of two vats of liquid, connected via a small passage (Figure 4). In this passage separating the two bodies of liquid is a cross-linked hydrogel sample (diameter = 15 mm, thickness = 1.5 mm). The device is clamped tightly in the middle, which can be separated to allow you to insert and remove the hydrogel. This passage area that contains the hydrogel and connects the two 100 mL bodies of liquid has a cross-sectional area of 0.785 cm². The cross-linked GelMA/HAMA samples were prepared at 0.12 wt% LAP, with irradiation energy of 408 mJ over 60 seconds using the 400 nm light source. Chamber one was loaded with 50 mL of glucose solution (12 mM) in PBS with 0.05 wt% sodium azide, and chamber 2 with 50 mL of PBS with 0.05 wt% sodium azide and a magnetic stirrer bar was used to circulate the solution within the chamber 2. After the hydrogel was clamped between the two vats, fluid was added to one side first for five minutes. This ensured that there were no leaks through or around the hydrogel and that any solute that crossed into the other vat went through the

hydrogel. 110 μ L aliquots were taken from chamber two at various time intervals for 24 hours. The concentration of glucose in the aliquots was measured by an Amplex[®] Red Glucose/Glucose Oxidase Assay (Thermo Fischer) according to manufacturer's protocol.

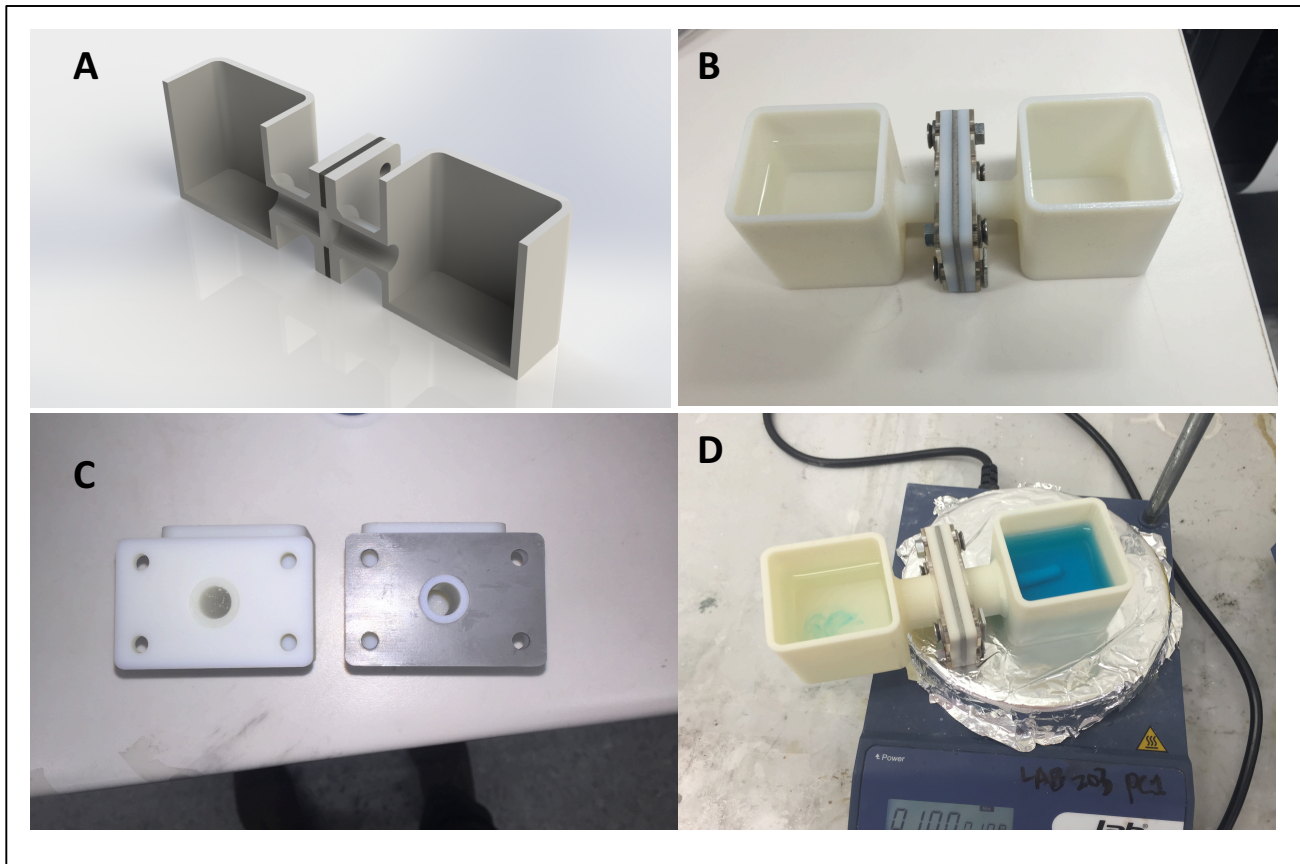


Figure 4. Diffusion chamber. A) Render of the custom designed diffusion chamber. Designed in Solidworks by Adam Taylor and printed on the Connex inkjet printer. B) Chamber assembled. C) Cross-section of chamber where the hydrogel sample is loaded. D) Example of a gradient created between the two chambers with fluorescence.

Briefly, the samples taken from chamber 2 were diluted 200 times and mixed with a working solution of 100 μ M Amplex[®] Red reagent, 0.2 U/mL horseradish peroxidase (HRP) and 2 U/mL glucose oxidase. The reaction was incubated at room temperature for 30 minutes and protected from light. Fluorescence was then

measured with a fluorescence microplate reader using excitation at 535 nm and fluorescence detection at 560 nm. A standard curve was established using standard glucose solutions and used for quantification of the amount of glucose in each sample.

2.6 Co-axial printing

The extrusion rates of the core and shell (0.4 mm and 1.0 mm radius respectively) can be varied independently via the display unit and the feed is initiated by a foot pedal. An external 400 nm light source (OmniCure 4000) is mounted on the side of the Biopen in order to initiate photo-crosslinking after extrusion of the GelMA/HAMA ink.

GelMA/HAMA was loaded into two 3 mL cartridges suitable for the Biopen. Blue dye was added to the core cartridge at ~1 wt% to aid in visualization. Photo-initiator was added to the shell at a concentration of 0.12 wt%. These cartridges were placed on ice in order to cool them adequately prior to printing.

In order to control the gap distance and speed of the Biopen, it was attached to an XY plotter (Figure 3). A Me3, ME2 FDM printer was modified by removing the plastic extrusion head and adding a custom 3D printed Biopen holder. The Biopen was placed into the holder and the nozzle's distance to the substrate was calculated. The gap distance was set at 0.25 mm and the speed at 7.5 mm/s.

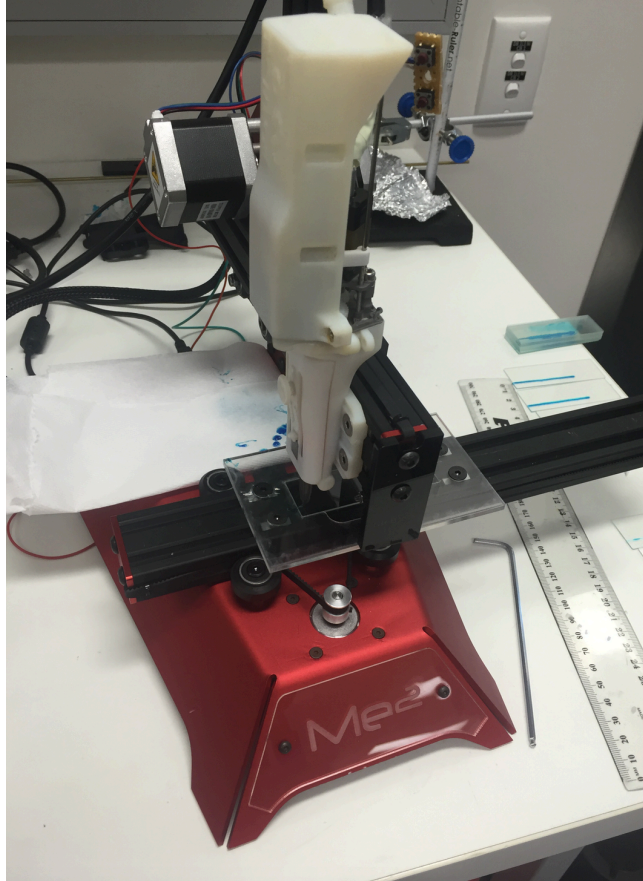


Figure 5. Biopen attached to XY plotter in order to control the rate of movement and gap distance.

As the Biopen has arbitrary units for extrusion, the flow rate was determined by extruding water at various extrusion rates and core: shell ratio's in order to determine if there was a linear increase in extrusion and if the core and shell extrusion was even.

Lines were printed at the extrusion setting of 8 (0.25 mL/min) and 12 (0.36 mL/min), while the core: shell ratio was varied at 50:50, 25:75 and 10:90. The extruded ink was cross-linked for 60 seconds using the Omnicure 400nm light, at a distance of 5 cm, with the total energy output being 408 mJ. The extruded lines were imaged under a microscope and the strut width measured.

3 Results and discussion

3.1 Material functionalization and characterization

Firstly, methacrylic anhydride was employed for substitution of gelatin with methacryoyl groups via the formation of amide bonds, as shown in Figure 6. The level of methacrylic anhydride added affects the degree of substitution and consequently the strength of the scaffold. Past literature by Fathi *et al.* suggests that between 50-70% modification is appropriate (Fathi et al., 2014).

The degree of methacrylation of GelMA was determined by ^1H NMR spectroscopy recorded at 40 $^{\circ}\text{C}$ (128 scans). Figure 7 demonstrates the NMR spectra of both gelatin and GelMA. The green region represents the phenylalanine signal (6.9 – 7.5 ppm), which was used for normalization. The grey region represents the lysine group (2.8 – 2.95 ppm), which underwent methacrylation. Two peaks are present in the GelMA sample (5-6 ppm) that corresponds to the vinyl protons of methacryoyl side chains. The degree of methacrylation was calculated to be 60%, according to the following formula.

$$\text{Degree of modification} = \left(1 - \frac{A(\text{Lysine in GelMA})}{A(\text{Lysine in unmodified gelatin})}\right) \times 100 \quad \text{Equation 6}$$

$$\text{Degree of modification} = 60\%$$

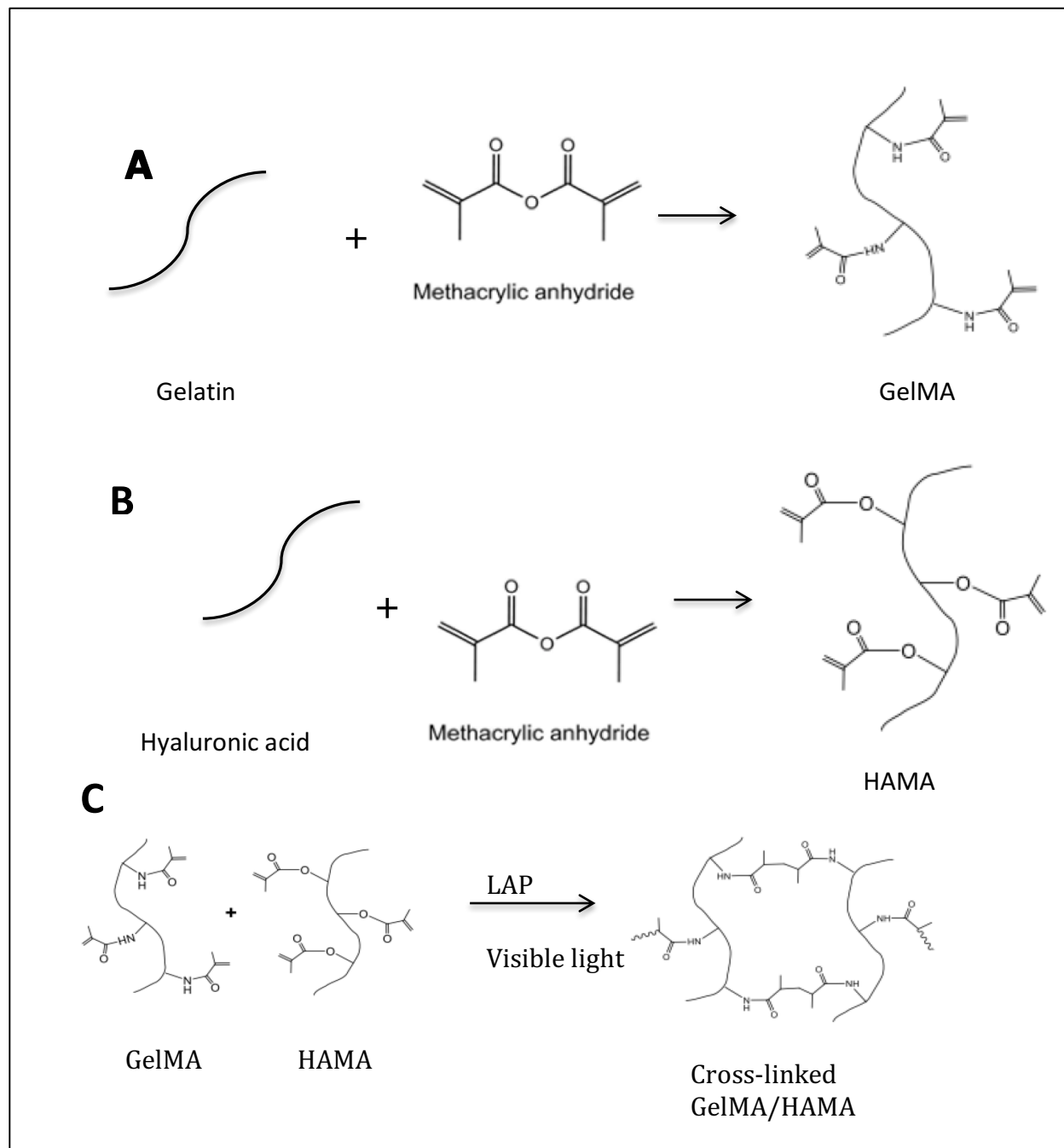


Figure 6. Schematics of (A) methacrylation of gelatin to form gelatin methacrylamide (GelMA), (B) Methacrylation of hyaluronic acid to form HAMA and (C) LAP- initiated photo-crosslinking process of GelMA/HAMA.

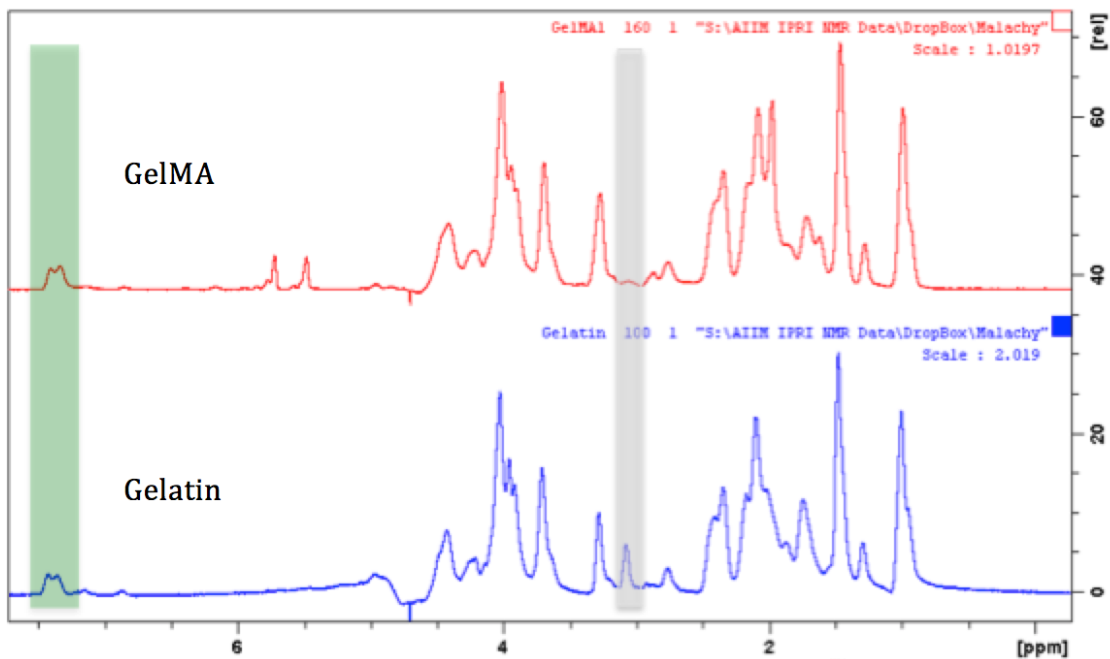


Figure 7. ¹H-NMR spectra of gelatin and GelMA. The green region represents the phenylalanine signal (6.9 – 7.5 ppm) and the grey region represents the lysine group (2.8 – 2.95 ppm).

3.2 Ink characterization

Printing of hydrogels has become an increasingly attractive process in biomedical research. The literature stresses that a greater understanding of the gels flow properties is critical in order to create a gel that is both capable of being printed at fine resolutions and remain a suitable carrier for cells. Rheological analysis of the GelMA/HAMA ink allows us to understand the flow properties of the material. This examination of the ink characteristics enables us to understand how the ink behaves while being extruded from the co-axial Biopen system.

In rheology, G' represents the storage modulus of a sample, that is the forces that hold the material together, while G'' represents the loss modulus. When the storage modulus is greater than the loss, the material exists as an elastic gel/solid, and when G'' dominates the material is described as a viscous liquid. For fine resolution printing of hydrogels, a storage modulus of 900 Pa is required (Mondal et al., 2016).

In this study, polymer ink was prepared containing 10 wt% GelMA and 2 wt% HAMA. Like gelatin, the GelMA aqueous solution at 10 wt% undergoes a solid-gel transition when cooling from 37°C to 5°C (Figure 8A). The thermo-gelling property of GelMA provides a means to engineering of the viscoelastic properties and hence the printability of the GelMA/HAMA ink. A temperature scan was performed in order to determine the temperature range in which the ink can be printed with high shape fidelity. Figure 8C shows that at temperatures below 17°C, GelMA/HAMA's modulus is >900 Pa. The combination of HAMA, which has a modulus independent of the temperature, and GelMA which alone has a low storage modulus, combine to produce a bioink which has an appropriate modulus for printing below 18°C (Figure 8A and B). As the current design of Biopen does not have any mechanism of temperature control, it is suggested that the ink should be taken directly from the fridge and loaded into the pen for immediate extrusion. As such, all further rheological measurements were conducted at 5°C. The temperature scan results suggest there is a need for further modification of the existing biopen with temperature control capacity and/or ink optimization to improve the gelation capability at room temperature.

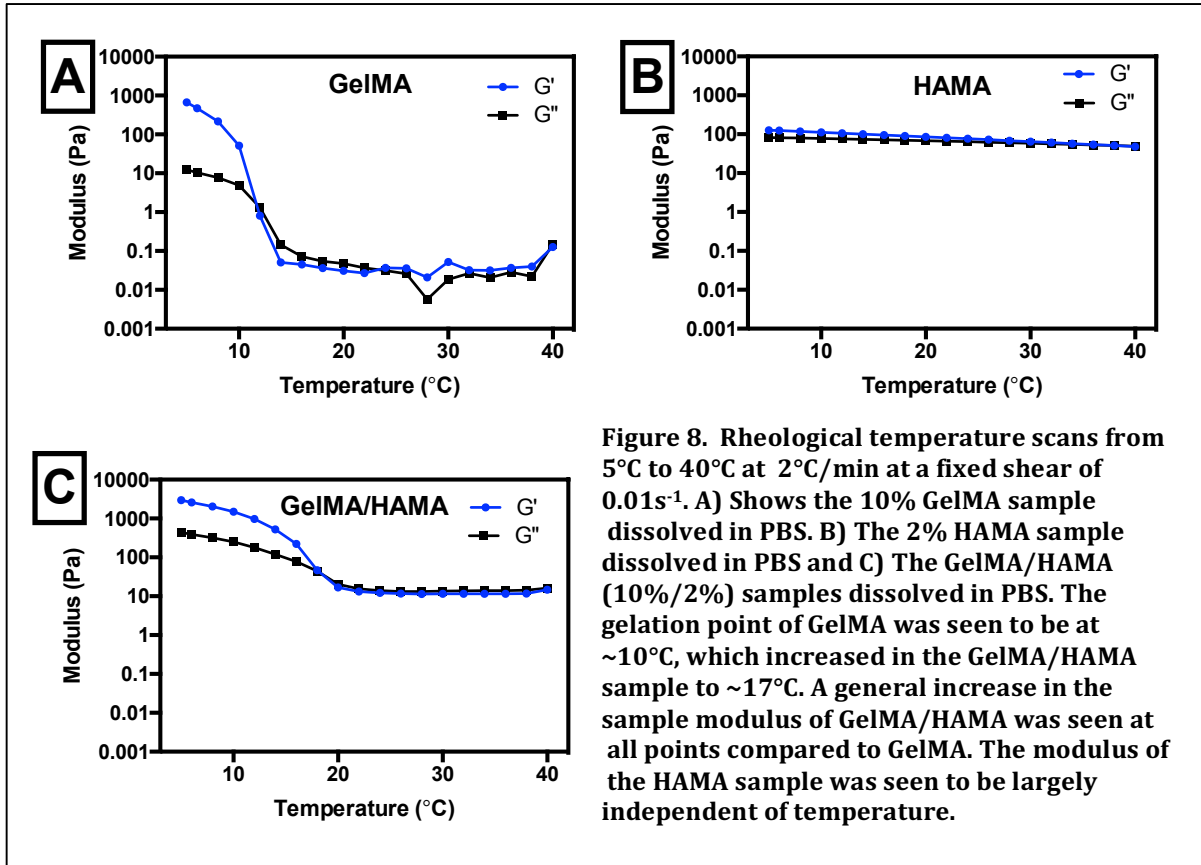


Figure 9A shows that GelMA/HAMA sample has a large linear viscoelastic region (LVR), continuing up until 20% strain. This large LVR indicates that the gel is tough and confirms that we can perform the frequency sweep at non-destructive stress level of 1% strain. This frequency sweep (Figure 9B) classified the GelMA/HAMA as a solid-like gel at the testing temperature (5°C). The phase angle of ~10° indicates that the material is elastic like, rather than viscous.

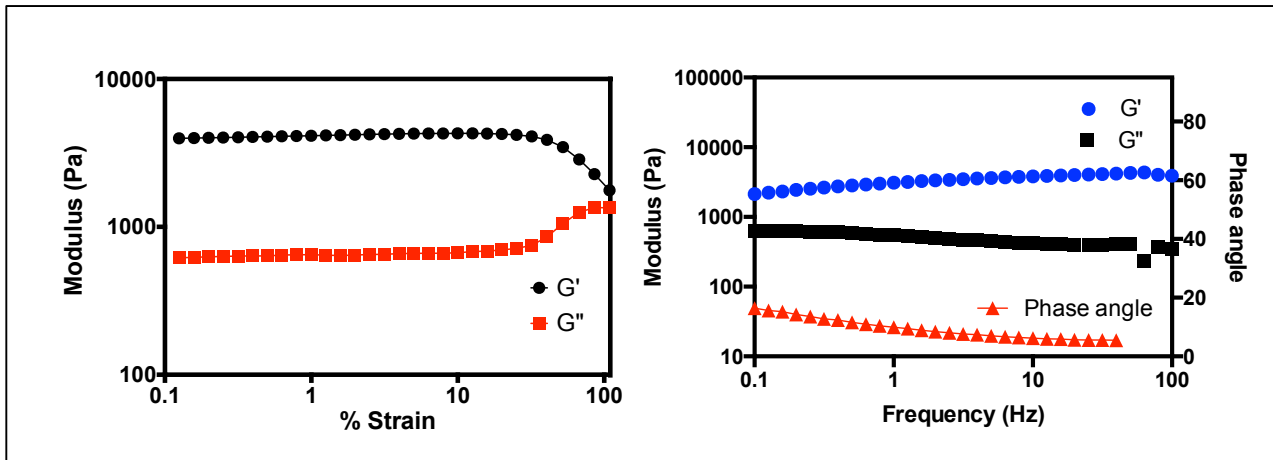


Figure 9. Rheological oscillation scans of GelMA/HAMA at 5°C. A) Shows the strain sweep from 1-100% strain, (Frequency fixed at 1 Hz) with a large linear visco-elastic region up until ~20%. B) Shows the Frequency scan from 1-100 Hz (Strain fixed at 1%).

The most important properties an ink should have for extrusion printing include shear-thinning and fast self-recovery. Both of which were demonstrated in the GelMA/HAMA ink. A shear rate sweep (Figure 10A) was conducted to determine the viscosity of the sample at various level of shearing. From this it is evident that the viscosity decreases as the shear rate increases, proving that the sample is non-Newtonian and undergoes shear-thinning (pseudoplastic). This shear-thinning behavior can be described by the power-law relationship. By fitting the viscosity-shear rate curve with the power-law, n , the shear-thinning exponent, was determined to be 0.054.

$$\eta = K\gamma^{n-1} \quad \text{Equation 7}$$

η = Viscosity (Pa.s)

γ = Shear rate (s^{-1})

K = Viscosity at a shear rate of $1 s^{-1}$

The viscosity and flow rate have a direct impact on the stress that the gel experiences upon extrusion through a nozzle. In order to calculate the maximum shear rate that the ink is subjected to during extrusion, and consequently the viscosity, the following equations have been used.

For Newtonian fluids: shear rate at the wall, $= \frac{4Q}{\pi R^3} = \frac{8V}{D}$ Equation 8

For non-Newtonian power-law fluids (Saffarian et al., 2015), the Rabinowitsch equation, $\gamma = \frac{4Q}{\pi R^3} \cdot \frac{3n+1}{4n}$ Equation 9

Where Q is volumetric flow rate, R is Radius of the nozzle, V is Velocity of extrusion, D is Diameter of the nozzle, and n is the shear-thinning exponent, obtained by fitting the viscosity/shear rate curve to a power law.

Equation 8 represents the shear stress experienced by a Newtonian fluid. By combining Equation 8 with the Rabinowitsch correction factor (Saffarian et al., 2015), we can determine the shear stress experienced in a non-Newtonian fluid using Equation 9. Based on the Law of the Wall principle, the fluid near the wall of the tube moves the fastest and thus experiences the highest level of stress, when compared to the slower moving fluid near the center of the tube. This equation calculates the stress at the walls, which is the highest in the nozzle. If the cells can survive in this high stress environment, they can survive anywhere in the nozzle (Nair et al., 2009). For example, when the ink is printed through the 400 μm biopen core nozzle at a rate of 0.24 mL/min, the calculated maximum shear rate was 41.1 s^{-1} , which correlates with a viscosity of 15.4 Pa.s. Under these conditions, the ink viscosity is about three orders of magnitude lower than that observed at a low shear rate ($\leq 0.1 \text{ S}^{-1}$).

In bioprinting, shear-thinning is preferred as this enables extrusion of filaments at low nozzle pressure so as to protect cells from physical stress during printing. Shear-thinning is often seen in polymer solutions, as a result of shear-induced reorganization of polymer chains.

Another critical requirement of a bioink is rapid self-recovery after extrusion. As the viscosity of the ink decreases during extrusion, it needs to increase quickly upon extrusion so that it can maintain its shape. A series of strain intervals were applied to the sample in order to simulate and examine the materials recovery. A high strain (100%) was applied in order to disrupt the inks internal network, followed by a low 1% strain used to examine the reorganization of the materials internal network. These intervals were performed three times as seen in Figure 10B and C. The GelMA/HAMA exhibited rapid self-recovery, with the modulus increasing 5 fold (1000 to 5000 Pa) returning to its original range within 10 seconds of experiencing the disruptive high strain. The rate of recovery remained consistent over the three cycles. This is favorable for extrusion printing as it allows the printed structures to retain their resolution, a critical requirement of core-shell structures.

As the viscosity of the gel varies at different shear rates, it is important to understand the level of applied stress required to initiate gel flow. The critical level of applied stress required in order to initiate flow is termed the yield point (Figure 10D). At stresses below the yield point the material absorbs the applied energy, however at the yield point the material begins to flow. The rapid decrease in viscosity at ~ 900 Pa.s indicates that the gel can no longer withstand and absorb the applied stress and begins to flow. The yield stress is determined to be around 1000 Pa.

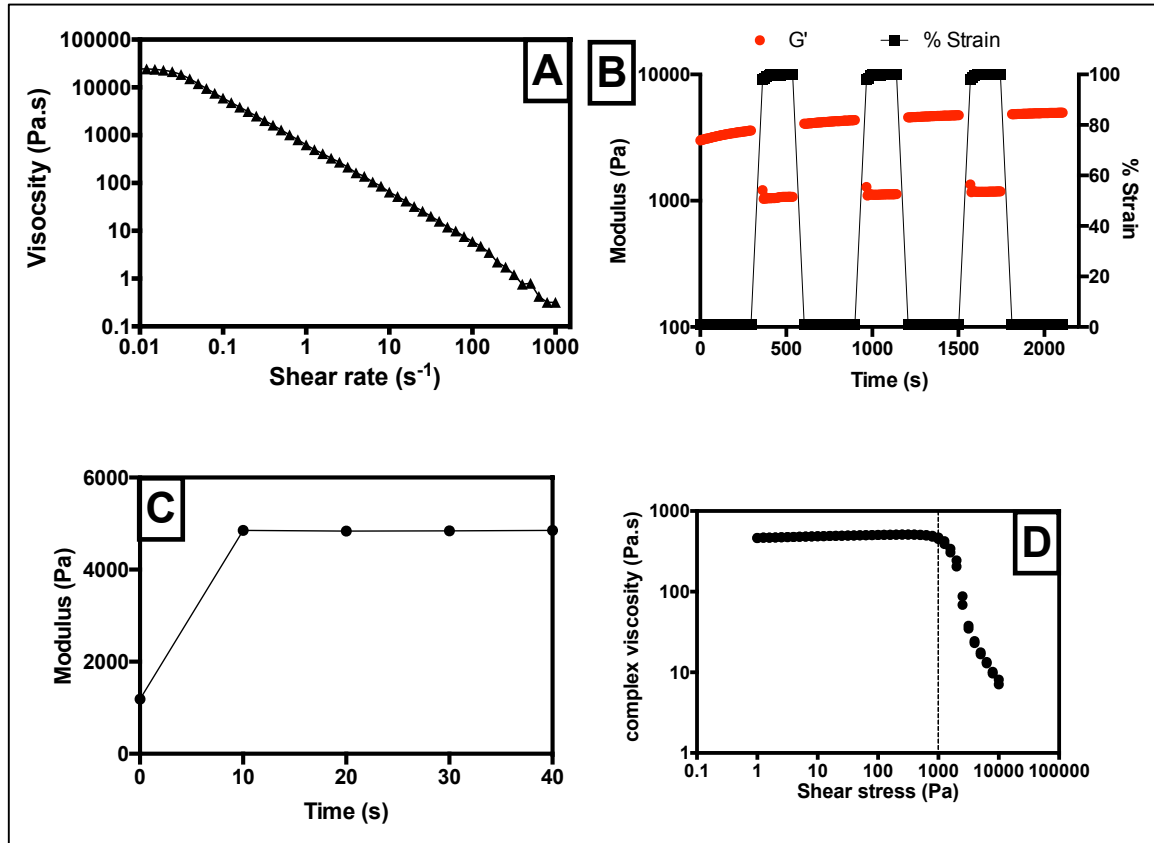


Figure 10. Rheology scans performed with GelMA/HAMA at 5°C. A) Shows the shear-thinning effect seen during the shear rate scan, with the viscosity decreasing as the shear rate increases. B) The step strain graph using a low strain of 1% and a high strain of 100% to disrupt the internal network of the GelMA/HAMA. C) Shows a close up of the recovery of the ink in B after the high strain is released, with the sample modulus increasing 5 fold to return to its resting level within 10 seconds. D) Shows the yield point of GelMA/HAMA (~900 Pa).

These results highlight that the GelMA/HAMA is a suitable material for extrusion printing. The printing range of 5°C-17°C has been identified. The material undergoes shear-thinning in response to an applied shear rate. This means that the viscosity decreases upon extrusion, exposing the encapsulated cells to less stress. Additionally, the material was seen to have rapid self-recovery after extrusion. These properties are favorable as the material can maintain its shape after experiencing the thinning during extrusion, critical to achieving the core-shell structure.

3.3 Photo-induced crosslinking kinetics of ink

3.3.1 Light attenuation

The absorbance of the LAP photo-initiator was measured in PBS and in the GelMA/HAMA gel to determine the effect that the GelMA/HAMA ink had on 400 nm light transmittance. At 400 nm the molar absorptivity coefficient for LAP in PBS was calculated as $72.0 \text{ L mol}^{-1} \text{ cm}^{-1}$ and $71.5 \text{ L mol}^{-1} \text{ cm}^{-1}$ in the GelMA/HAMA sample. The opaque GelMA/HAMA showed similar absorbance values as PBS, with 93.5% of light penetrating 1 mm and the $T_{50\%}$ occurring at 10.5 mm. As the printed structures are generally $<1 \text{ mm}$, the decrease in transmittance is negligible. The concentration of Lap affected the transmittance in GelMA/HAMA, as the 0.06 wt% had $T_{50\%}$ of 20.5 mm while the 0.12% LAP sample absorbed more light, with a $T_{50\%}$ of 10.5 mm. Overall, this high transmittance suggests that the structures will undergo uniform crosslinking, which ensures even mechanical and diffusion properties in the gel.

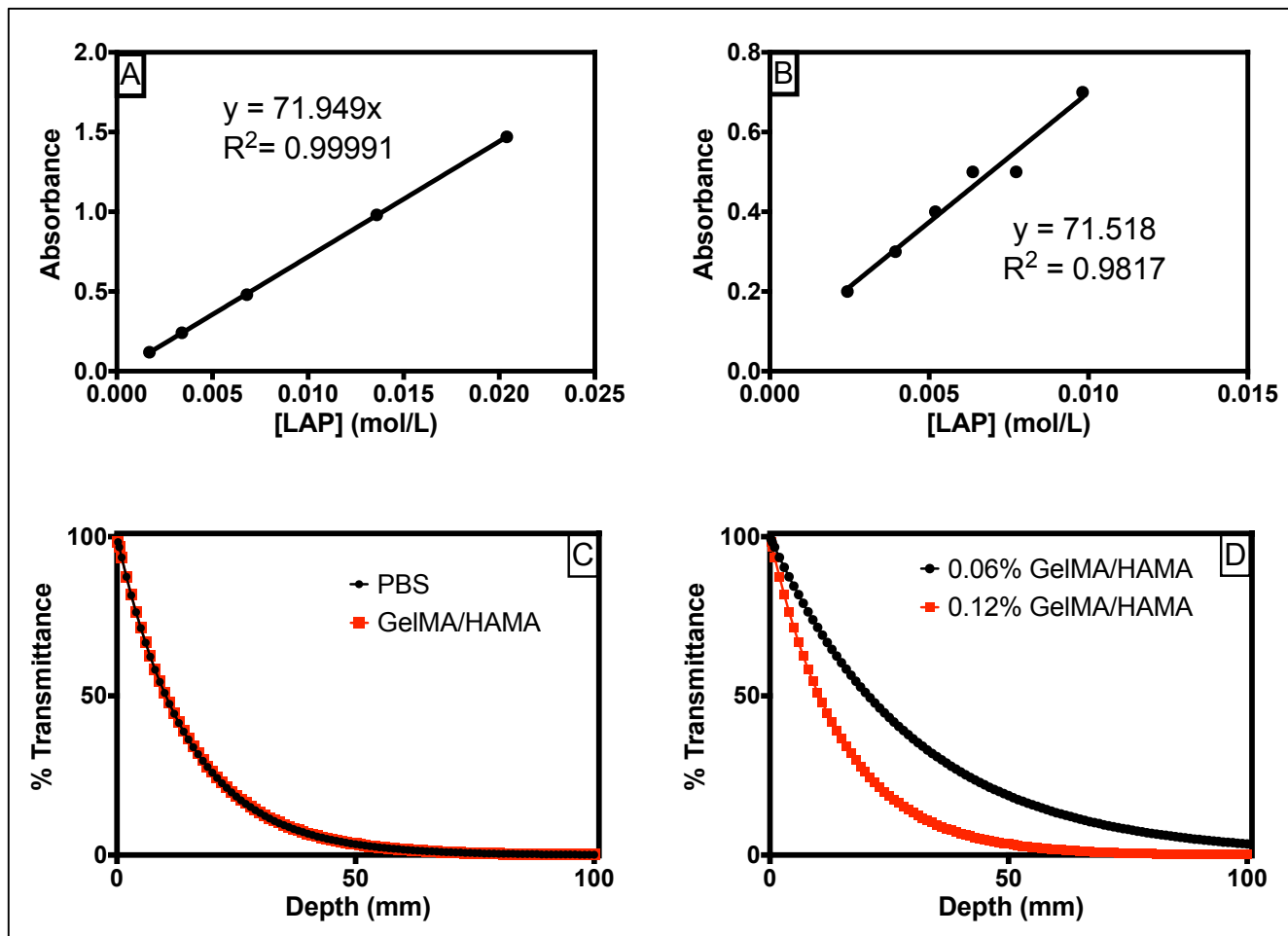


Figure 11. A and B) UV-vis absorbance at 400nm of LAP dissolved in PBS and LAP in GelMA/HAMA. C) 400 nm UV light penetration depth in PBS and GelMA/HAMA with 0.12% LAP, calculated by using the Beer-lambert equation with the UV-vis data. D) Penetration depth of 400 nm UV light in GelMA/HAMA with 0.06 wt% and 0.12 wt% LAP.

3.3.2 Crosslinking kinetics

The modulus of the GelMA/HAMA ink was measured during crosslinking by *in situ* UV rheology. To examine the rate of light initiated crosslinking, two photo-initiator concentrations and three light intensities were applied over a 60-second exposure time (Figure 12). All conditions saw instantaneous crosslinking (at 60 seconds as the light was applied) as well as constant rates of crosslinking throughout the period of light exposure, calculated with a linear regression analysis of the crosslinking region (60-120 seconds) (Figure 12). The rate of cross-linking (Pa/s) (Table 6) was seen to increase with the concentration of LAP as well as with the increase in intensity of applied light. This is likely a result of increased free radical production, initiating crosslinking between the GelMA/HAMA molecules. After the light source was removed (120 seconds), the modulus of all samples was seen to continue to increase, but at a much lower rate. This is likely a result of remaining free radicals continuing to react. Past studies have shown that Irgacure 2959 can experience lag in its crosslinking, as oxygen in the sample had to be removed by reacting with the free radicals before the structures would crosslink (Klotz et al., 2016). This study found that LAP underwent instantaneous crosslinking. Additionally, the time to gelation was 10 times faster with the LAP photo initiator compared to Irgacure 2959 at 365 nm (Klotz et al., 2016).

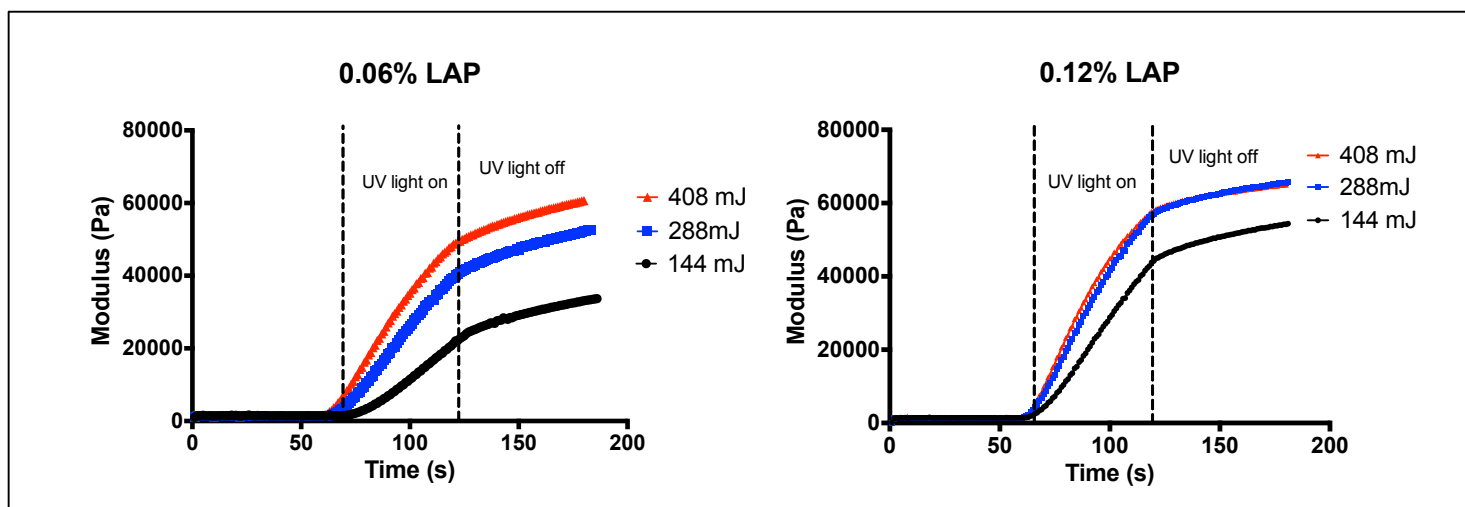


Figure 12. Cross-linking kinetics of GelMA/HAMA. Two different concentrations of LAP were used (0.06 and 0.12 wt%) and three different intensity's of light were applied (144, 288 and 408 mJ). A 60 second equilibration period was allowed before the light was applied for 60 seconds, and a 60 second post exposure period is also shown. Run 1 is shown, which is representative of the overall trend seen.

Table 6. Rate of UV-crosslinking with the LAP photo-initiator and 400 nm light. Two different photo-initiator concentrations were used (0.06 and 0.12 wt%) and three levels of irradiation energy (127, 255 and 361 mJ/cm²).

[Photo-initiator] wt%	Light exposure (mJ/cm ²)	Rate of crosslinking (Pa/s)
0.06%	127	330
0.06%	255	633
0.06%	361	786
0.12%	127	810
0.12%	255	925
0.12%	361	942

From Figure 13, we can see the modulus of the samples immediately post-curing (120 seconds). Here, the modulus was seen to be dependent on the concentration of photo-initiator and the intensity of light. Studies from *Klotz et al.* 2016 have shown that photo-initiators cause cell death, because of free radical production and photo-initiator cytotoxicity (Klotz et al., 2016). Additionally, while studies show that 400 nm light used with LAP does not affect cell viability, the long-term effects of UV exposure on early stage cells is not fully understood and damage to DNA and proteins could occur, so minimising the exposure is of importance. By understanding the rate of crosslinking, we can determine the lowest concentration of photo-initiator required to achieve appropriate mechanical properties as well as the duration and intensity of light that is required.

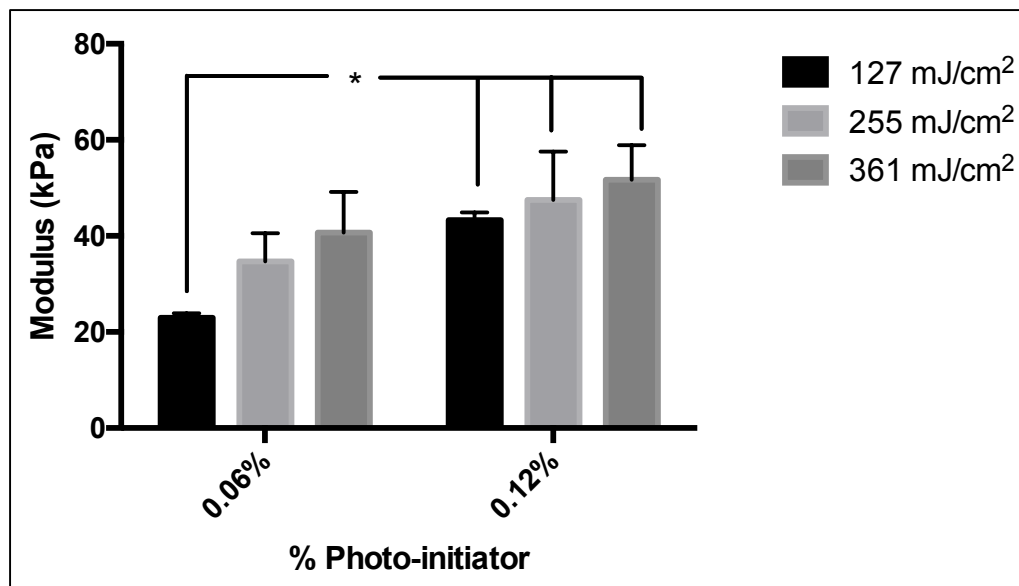


Figure 13. Modulus of samples immediately after UV-crosslinking. The low concentration sample that received low light intensity had a significantly lower modulus than all samples that received the high concentration LAP.

3.4. Physiochemical characterization of the photo-cross-linked GelMA/HAMA hydrogel as shell component

3.4.1 Free polymer loss

As shown in Figure 14, all samples lost between 8 and 12 wt% of their original mass, indicating that 88-92 wt% polymer (GelMA or HAMA) was cross-linked. The low concentration photo-initiator (0.06 wt%) samples generally lost more free polymer (10-12 wt%) than the high concentrations group, indicating that they had a greater percentage of uncrosslinked polymers. Within this low photo-initiator concentration group, as the irradiation energy increased, the samples lost less free polymer (Figure 14), suggesting that the more intense the light, the more crosslinking that occurs, consistent with Figure 13. The higher concentration photo-initiator (0.12 wt%) generally lost less polymer (8-9 wt%), however varying the light intensity did not appear to affect the amount of polymer lost.

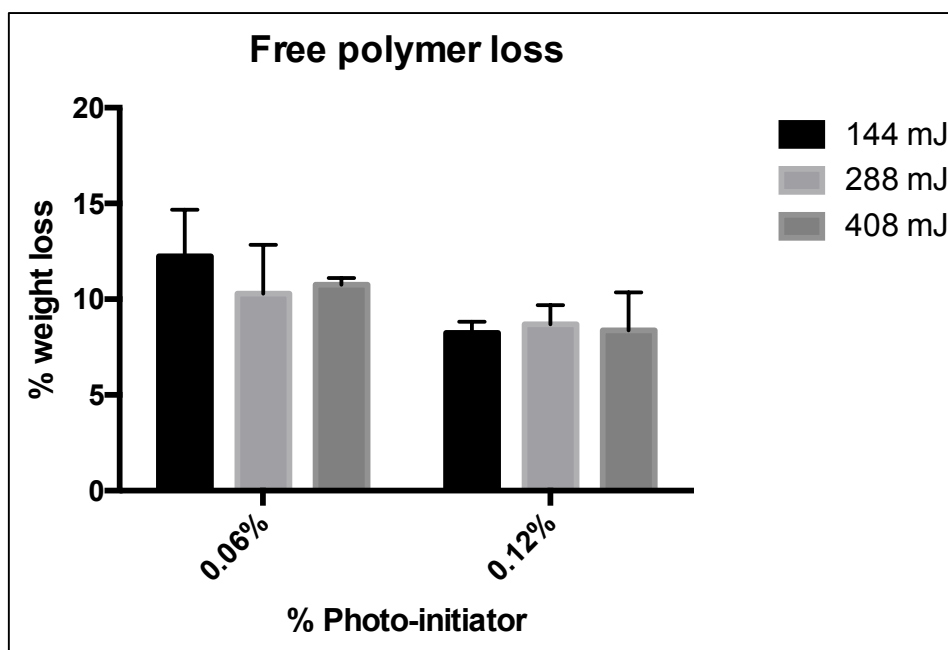


Figure 14. Free polymer loss of the cross-linked GelMA/HAMA prepared at different LAP concentration and/or irradiation energy level, respectively

3.4.2 Equilibrium water content

All the samples were freeze dried prior to the water uptake study. Figure 15 shows that all samples were able to uptake water ~15 times their dry polymer weight, except for the samples cross-linked at 0.06 wt% LAP and with the lowest light intensity (144 mJ) which held significantly more water. This suggests more than 93 wt% equilibrium water content in the GelMA/HAMA hydrogels.

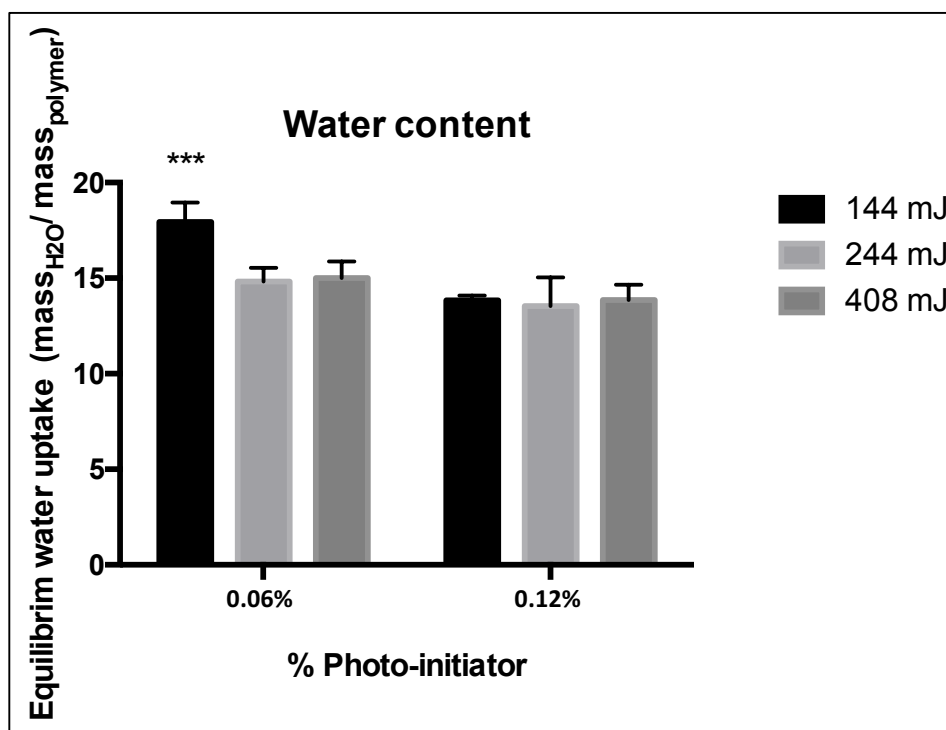


Figure 15. Equilibrium water content of the cross-linked GelMA/HAMA prepared at different LAP concentration and/or irradiation energy level, respectively.

3.4.3 Gel mechanical properties

In order to examine the mechanical properties of the GelMA/HAMA, micro-indentation was performed. As shown in Figure 16, all samples displayed a Young's

Modulus of about 150 kPa, except for the group that was cross-linked at the lower LAP concentration (0.06 wt%) and also received the lowest light energy (144 mJ). This group had a significantly lower Young's Modulus value of about 75 kPa ($p < 0.005$, Figure 16). This suggests that the Young's modulus of all scaffolds has reached the threshold of crosslinking, except for one group. The sample that received the low concentration photo-initiator (0.06 wt%) and was exposed to the low level of light irradiation (144 mJ) displayed significantly lower values of Young's modulus indicating possible incomplete cross-linking. This theory consistent with the water uptake data where the same sample also swelled significantly more than the others. These high modulus groups (150 kPa) are comparable to native articular cartilage 160 – 430 kPa, meaning that the scaffolds should be mechanically suitable for implantation (Woodfield et al., 2004).

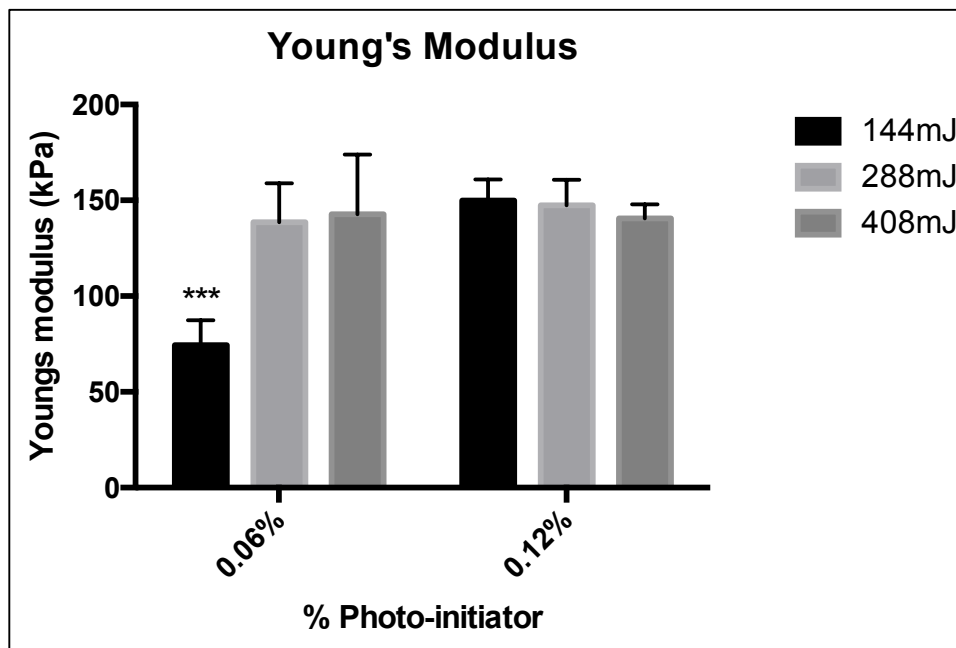


Figure 16. Young's Modulus of the cross-linked GelMA/HAMA prepared at different LAP concentration and/or irradiation energy level, respectively. The first sample (0.06 wt% LAP, 144 mJ light irradiation) sample had a significantly lower Young's Modulus than all other conditions ($p < 0.005$).

3.4.4 Diffusion characteristics

The movement of glucose (180 Da) through the cross-linked GelMA/HAMA hydrogel was examined. Glucose began to diffuse through the hydrogel after an average of 22 minutes. Using the equation from *Hannoun et al.* 1986 and *Teixeria et al.* 1994, the diffusion co-efficients were calculated (Hannoun & Stephanopoulos, 1986; Teixeira, Mota, & Venâncio, 1994). By calculating the lag time (time taken for glucose to cross the scaffold membrane into chamber 2) we can use the scaffold membranes thickness to calculate the diffusion co-efficient (equation 10). The mean calculated diffusion co-efficient was $4.06 \times 10^{-6} \text{ cm}^2 \text{ s}^{-1}$, standard deviation = 2.62×10^{-6} (64.67%), which is in line with current literature (Table 7). For example, the diffusion co-efficient in a 4% alginate/5% gelatin was $1.13 \times 10^{-6} \text{ cm}^2 \text{ s}^{-1}$, and 4% alginate solutions have been reported with $6.7 \times 10^{-6} \text{ cm}^2 \text{ s}^{-1}$ and $5.0 \times 10^{-6} \text{ cm}^2 \text{ s}^{-1}$ (Hannoun & Stephanopoulos, 1986; Longsworth, 1953; Marchioli et al., 2015). This relatively high rate of glucose movement is favorable for the co-axial printing system as it allows rapid transport of molecules through the shell into the core with the cells. By understanding the rate of solute movement through the gel, we can relate this to the thickness of the shell and consequently the level of nutrients that will reach the core.

$$Q_{ts} = \frac{ADC_1}{l} \left(t_s - \frac{l^2}{6D} \right) \quad \text{Equation 10}$$

Where,

Q_{ts} = Solute moved (mg)

A = Surface area (cm^2)

D = Diffusion co-efficient (cm^2/s)

C_1 = Concentration of diffusing molecule (g/L)

l = Length of diffusion disk (cm)

t_s = Time (seconds)

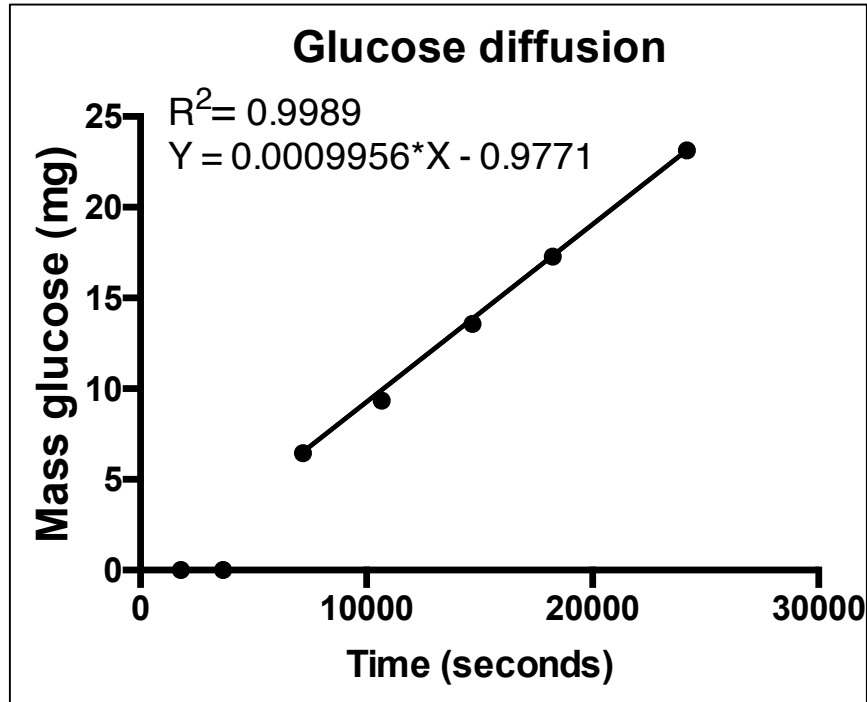


Figure 17. Glucose diffusion through the GelMA/HAMA hydrogel (0.12 wt % LAP and 408 mJ light irradiation exposure). After the initial lag period as the glucose was being absorbed into the gel the average rate can be seen in the equation. Run 1 shown is shown in this figure, which is representative of the trend seen. All triplicate runs shown in Table 8.

Experiment number	Diffusion co-efficient (cm ² /sec)	Lag time (seconds)
1	3.82E-06	981.4
2	6.80E-06	551.25
3	1.56E-06	2397.6
Average	4.06E-06	1310.07
Standard deviation	2.62E-06 (64.7%)	966.06 (73.74%)

Table 7. Summary of the glucose diffusion experiments performed in triplicate. The diffusion co-efficient of glucose and the lag time to initial movement are shown.

3.5. Co-axial printing

Preliminary printing was conducted in order to observe the flow properties that were examined in the rheology study. The Biopen was attached to the Me3D, Me2 X-Y plotter via a custom designed attachment. The X-Y plotter was programmed to move over a glass histology slide (nozzle distance to slide= 0.25mm) at a rate of 7.5 mm/s. The core has a radius of 400 μm , which is within the shell. Separating the core and the shell is a cylinder 200 μm thick. The shell is 600 μm from the outer wall of the core to the inner wall of the shell. The biopen has arbitrary extrusion units, so the flow rate was calculated experimentally. By extruding the core individually, the shell individually and both the core and shell together, the overall flow rate was varied as well as the core-shell ratio in order to determine if these variables resulted in a linear increase in extrusion. Overall extrusion settings of 5, 10 and 15 were used, and the core-shell ratio was varied from 0% core, 100% shell, to 100% core, 0% shell in increments of 25%. Water was extruded which was then weighed to determine volume (table 8). Figure 18 shows consistent extrusion, which increased in a linear manner with the flow setting and core-shell ratio. Each flow setting unit equated to an extrusion rate of $\sim 400 \mu\text{L}/\text{min}$.

In order to examine the printed lines, two extrusion rates were utilized, as well as three core-shell ratios, 50:50, 25:75 and 10:90. The sample was UV cross-linked at 400nm upon extrusion. Triplicates of each extrusion rate were completed. After the samples were printed, macroscopic and microscopic images were taken.

The shear thinning effect was noticed while printing. Initially, the GelMA/HAMA sample had a high viscosity and was slow to extrude. After some flow began, the sample experienced shear stress, its viscosity decreased and it began to flow more readily. In order to ensure a consistent viscosity and flow, extrusion was initiated before the Biopen was over the slide. The initial gel flow was wiped away from the nozzle with a paper towel, and once the pen was moving over the slide with a consistent flow the gel was allowed to extrude onto the slide. The fast thixotropic properties observed in GelMA/HAMA during the rheological study mean that if we

stop the flow, the gel's viscosity will recover quickly and the gel will be harder to extrude and will not drip out of the nozzle. Overcoming this initial resistance is key to ensuring a consistent line and core:shell ratio. These results are promising for the use of the Biopen in *in situ* extrusion of GelMA/HAMA for cartilage regeneration.

The higher extrusion rates produced larger diameter lines as expected, as more ink was extruded. Interestingly, as a larger ratio of shell was extruded the strut width increased as well, as seen in Figures 19 and 20. This is perhaps due to the GelMA/HAMA spreading out on the slide before it can be fully cross-linked. At a core-shell ratio of 50:50, the low extrusion setting of 8 (0.25 mL/min) produced lines that were significantly thinner than the high extrusion setting of 12 (0.36 mL/min) at core-shell ratios of 25:75 and 10:90 ($p < 0.05$). Looking at the cross sectional image in figure 20 we can see the core and shell profile. As the Biopen nozzle's were printed approaching the finest resolution the printer can achieve, small defects may be present, and consequently cause asymmetric structures.

Table 8. Biopen extrusion rates at various extrusion settings and core: shell ratios. Water was used and weighed assuming 1 mL = 1 g. The core:shell ratio was varied from 0% core to 100% core, and three extrusion settings were used.

Flow setting	5			10			15		
	Core ratio ($\mu\text{L}/\text{min}$)	Shell ($\mu\text{L}/\text{min}$)	Both ($\mu\text{L}/\text{min}$)	Core ($\mu\text{L}/\text{min}$)	Shell ($\mu\text{L}/\text{min}$)	Both ($\mu\text{L}/\text{min}$)	Core ($\mu\text{L}/\text{min}$)	Shell ($\mu\text{L}/\text{min}$)	Both ($\mu\text{L}/\text{min}$)
0:100	0	147.7 ± 3	154.6 ± 8.9	0	294.9 ± 1.6	306.8 ± 5.6	0	432.2 ± 2.1	448.5 ± 11.5
25:75	39.3 ± 1.1	112.8 ± 2.0	151.7 ± 4.3	78.0 ± 1.5	242.4 ± 8.8	285.9 ± 17.7	104.8 ± 8.5	337.5 ± 5.6	439.3 ± 4.4
50:50	75.4 ± 0.9	75.3 ± 7.5	138.9 ± 6.9	144.9 ± 2.7	150.7 ± 1.8	292.7 ± 7.1	222.5 ± 1.3	223.9 ± 2.2	449.2 ± 5.2
75:25	111.9 ± 2.2	30.8 ± 1.4	149.1 ± 11.5	214.5 ± 4.5	75.0 ± 0.5	294.7 ± 3.4	334.5 ± 4.3	109.4 ± 4.2	440.6 ± 8.1
100:0	147.5 ± 22.6	0	153.7 ± 0.8	291.2 ± 0.9	0	298.3 ± 3.35	432.6 ± 13.7	0	446.9 ± 3.8

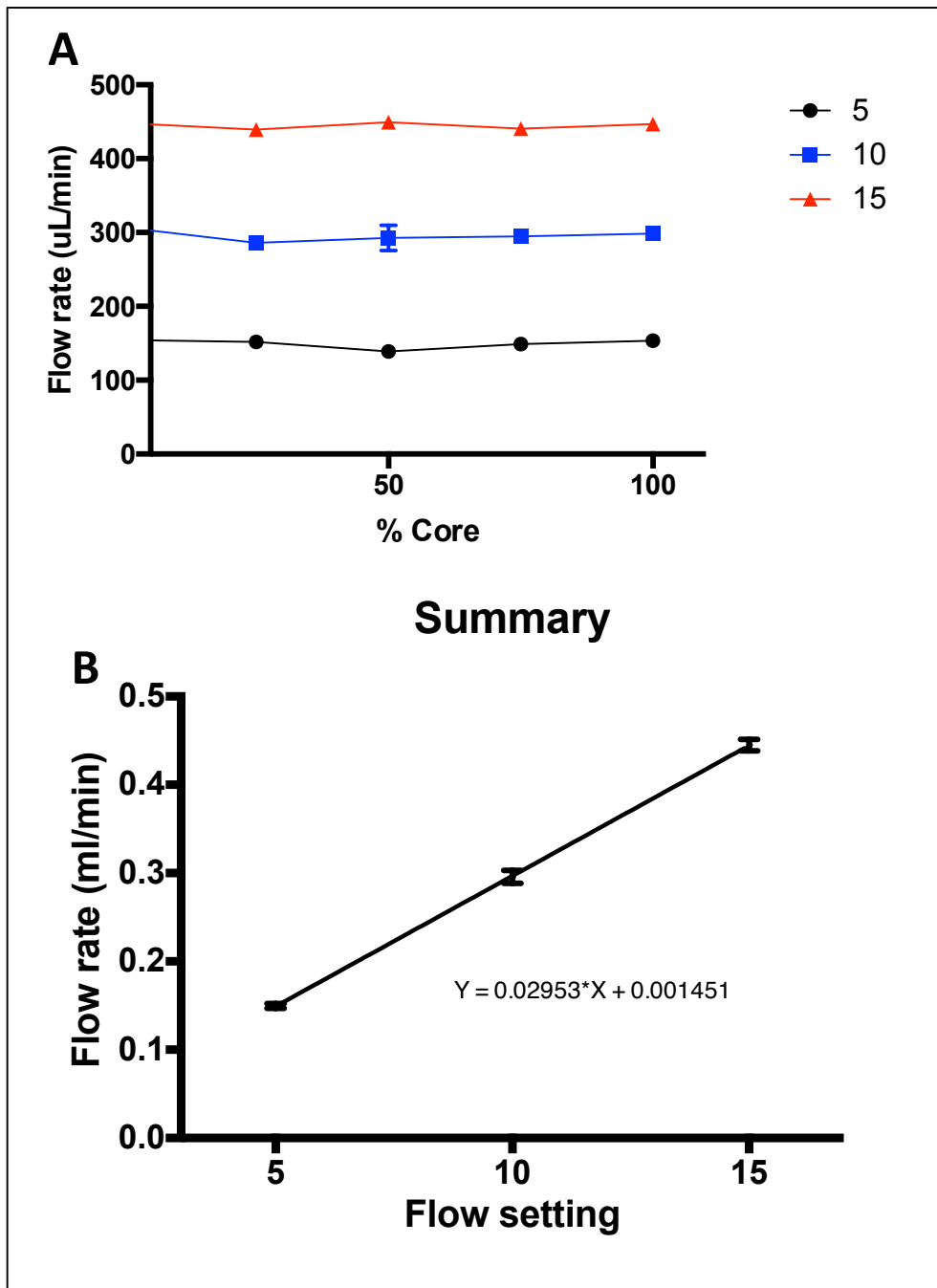


Figure 18. A) Biopen extrusion rates ($\mu\text{L}/\text{min}$) at varying core:shell ratios and the total extrusion settings 5, 10 and 15. B) Biopen extrusion rates at a 50:50 core:shell ratio, and the total extrusion settings 5, 10 and 15. The equation of the line is included so that exact volumetric extrusion rates ($\mu\text{L}/\text{min}$) can be calculated at any extrusion setting.


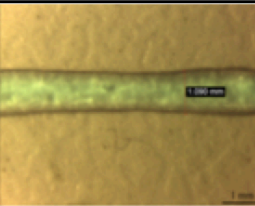
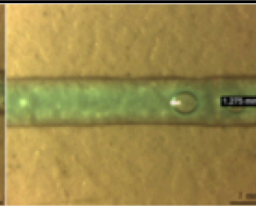
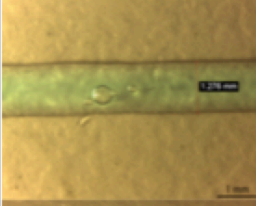
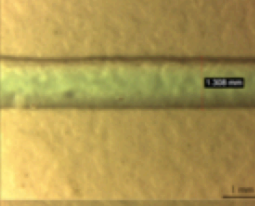
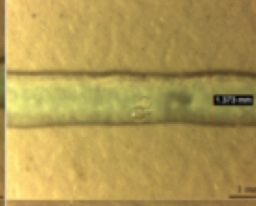
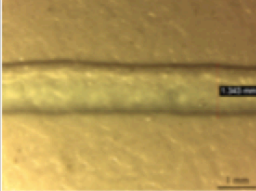

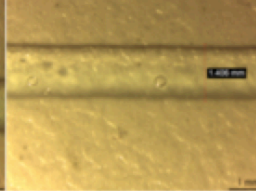
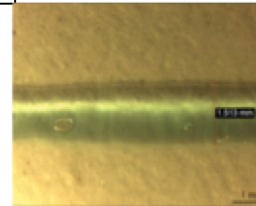
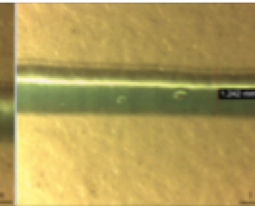
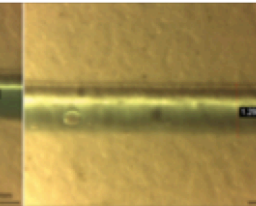
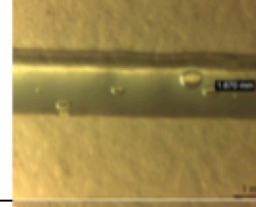

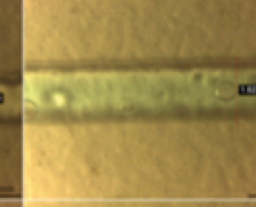
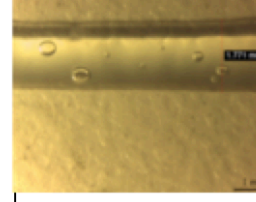
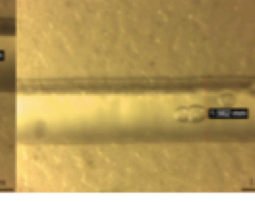
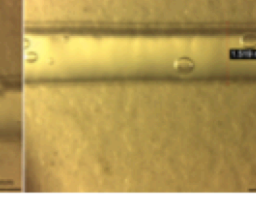
Core-shell ratio	Total extrusion rate = 8			Average strut width (mm)
50:50				1.14mm
25:75				1.32mm
10:90				1.39mm
Core-shell ratio	Extrusion Rate = 12			Average strut width (mm)
50:50				1.35mm
25:75				1.51mm
10:90				1.62mm

Figure 19. Microscopic images of extruded Biopen lines at a flow setting of 8 (0.25mL/min) and 12 (0.36mL/min), pen movement speed of 7.5mm/s and a gap distance of 0.25mm.

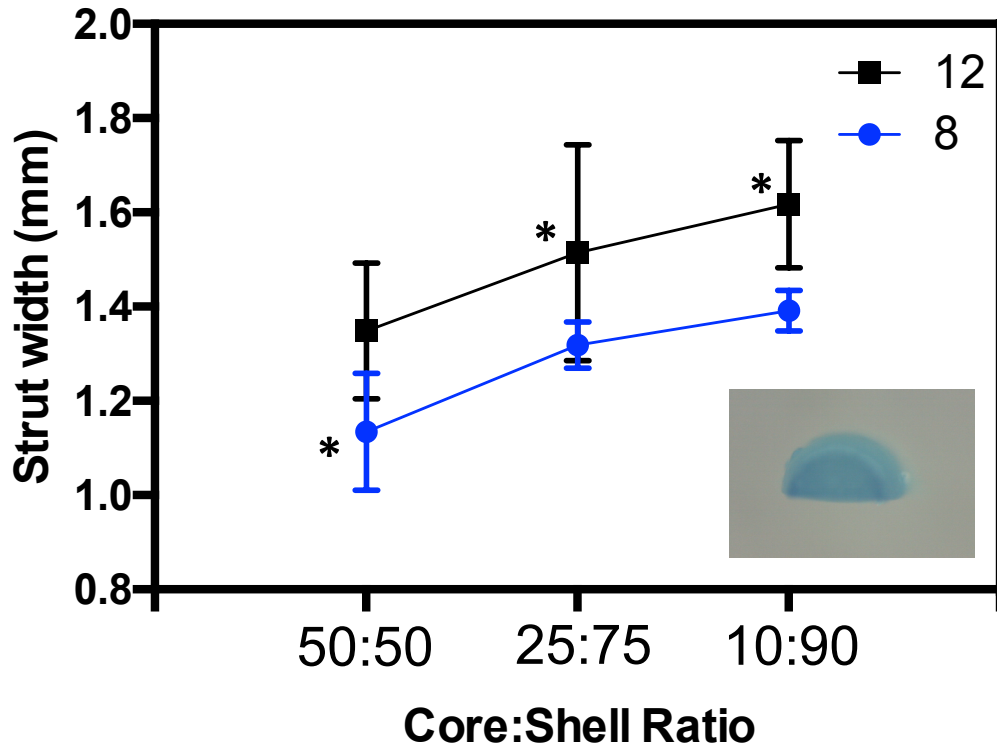


Figure 20. Strut width of the Biopen extruded lines measured from microscopic images. Strut width was seen to increase as the overall extrusion rate increased, but also as a high proportion of core was extruded. Lines printed at a 50:50 core-shell ratio at the extrusion setting of 8 (0.25 mL/min) were significantly thinner than lines printed at the high extrusion rate of 12 (0.36 mL/min) at core-shell ratios of 25:75 and 10:90 ($p < 0.05$). Inset is the cross-section of a co-axially extruded line, with the core-shell division visible. Printed at flow setting of '8' (0.25 mL/min) and a core:shell ratio of 50:50.

4.0 Conclusions

This project aimed to examine the gels inherent properties. GelMA is widely used in tissue engineering and its synthesis and characterization is established. Hyaluronic acid was methacrylated and added to the GelMA in order to improve its printability and direct cells towards chondrogenesis. By examining the flow properties, physical characteristics, mechanical properties, UV crosslinking kinetics, diffusion properties and co-axial printing properties we have a better understanding of the material and how it can be used for direct *in-situ* printing to regenerate articular cartilage. The GelMA/HAMA was seen to be printable, as it displayed shear thinning and fast self-recovery upon simulated extrusion. The printed scaffold achieved appropriate mechanical strength for use in joints such as knees, as seen with the high Young's Modulus of 150 kPa. Furthermore, while these printed scaffolds demonstrated adequate strength, glucose was also able to rapidly diffuse through the material. The rate of UV crosslinking with LAP was seen to be instantaneous and increase with the concentration of photo-initiator as well as the light intensity applied. The polymer held about 15 times its dry weight in water and lost about 10% of free polymer while washing. Using the current co-axial biopen (core surface area = 0.5 mm², shell surface area = 2.01 mm²), the general printing resolution achievable was seen to be 1 mm with the strut width increasing with the extrusion rate and as a higher proportion of shell was extruded. These results suggest that the GelMA/HAMA solution synthesized would offer an appropriate environment and strength for cell encapsulation and direct *in-situ* extrusion for tissue regeneration.

Appendix

The gelation point and Young's modulus of GelMA/HAMA samples was measured with the addition of nano-hydroxyapatite.

Nano-hydroxyapatite (Sigma Aldrich, <200nm) was added to the GelMA/HAMA samples at 0.5, 1.0 and 2.0 wt%. After dissolving, temperature rheology scans were performed from 45°C to 5°C (2°C /min) at a constant frequency of 1 Hz and strain of 1%.

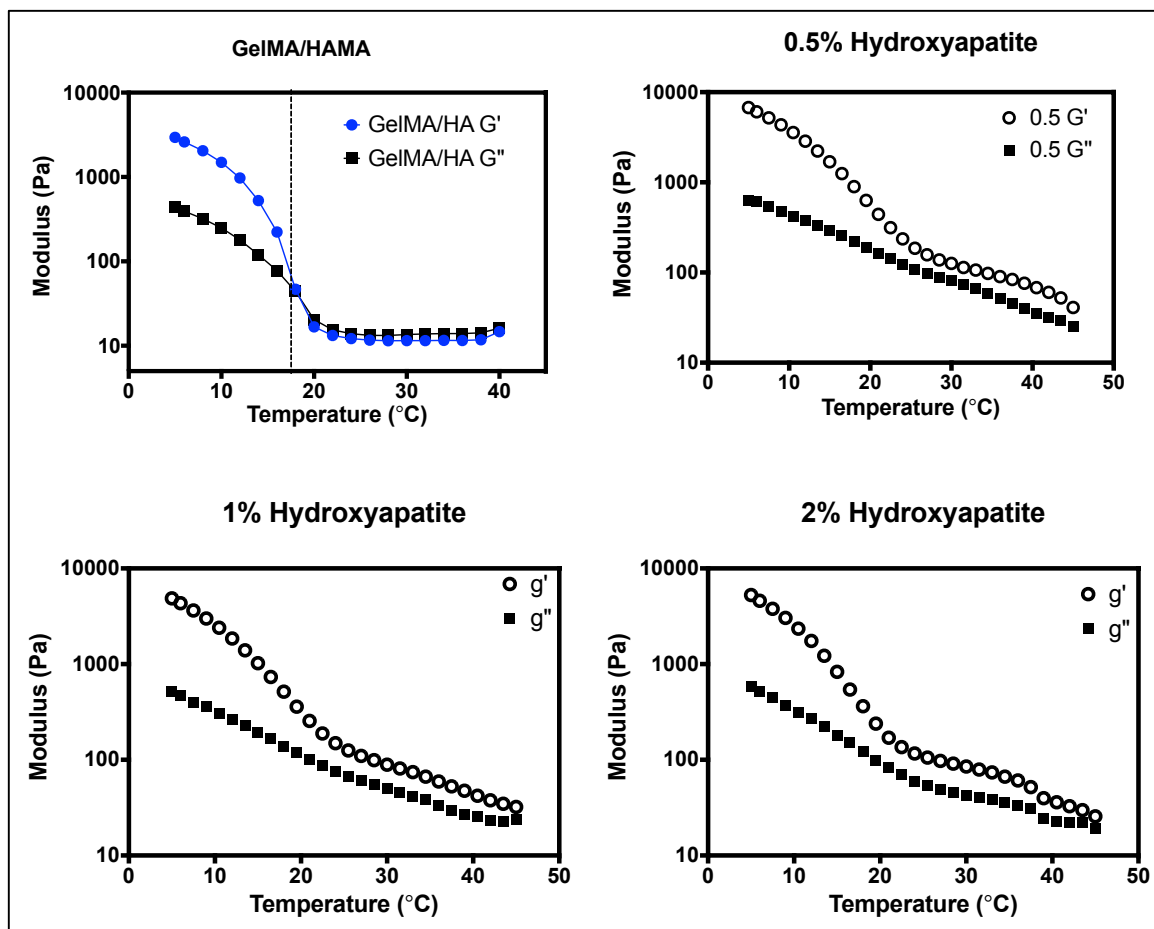


Figure 21. Temperature rheology scans with the addition of nano-hydroxyapatite. A control was used with no added hydroxyapatite and while three different amounts of hydroxyapatite were measured (0.5, 1.0 and 2.0 wt%).

A potential problem was highlighted that the gelation point was below the temperature in the operating room. If the ink is too warm it will not print properly, so the need to increase this gelation point or add a cooling temperature control to the Biopen is of importance. The addition of nanoparticles in the gel, such as nano-hydroxyapatite has been shown to assist in increasing this temperature. Further investigation of other Nano particles and their effect on the gels properties should be carried out. Additionally, in-depth printing and cell studies should be performed in an effort to push this project closer to real practical use.

The mechanical strength of cross-linked GelMA/HAMA with nano-hydroxyapatite was also examined using the same protocol as earlier. GelMA/HAMA samples were tested with 0, 0.5, 1.0 and 2.0 wt% nano-hydroxyapatite, at a fixed 0.2 wt% LAP content and 408 mJ light irradiation exposure.

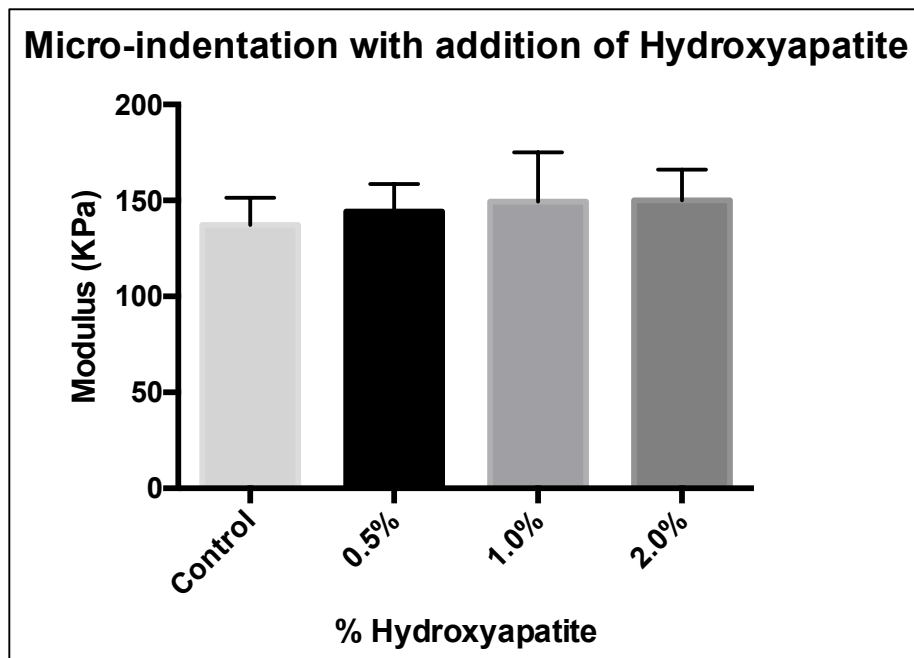


Figure 22. Young's Modulus of GelMA/HAMA samples with added nano-hydroxyapatite (0, 0.5, 1.0 and 2.0 wt%).

There was no significant difference in the Young's modulus between the control and any group with added nano-hydroxyapatite. This is not necessarily a negative effect, as if the gel becomes too stiff, cell growth will be hindered. So with the addition of nano-hydroxyapatite, we saw an increase in the storage modulus (G') of the material, and the Young's Modulus stay the same. The addition of hydroxyapatite improves printability but has no effect on the strength of the gel. Hydroxyapatite has been seen to promote osteogenesis, so it could be used in the bone-cartilage junction in severe articular cartilage defects. Addition of various nano-particles to could serve to optimize the bioink.

References

- Akmal, M., Singh, A., Anand, A., Kesani, A., Aslam, N., Goodship, A., & Bentley, G. (2005). The effects of hyaluronic acid on articular chondrocytes. *J Bone Joint Surg Br*, 87(8), 1143-1149. doi: 10.1302/0301-620x.87b8.15083
- Bian, Liming, Hou, Chieh, Tous, Elena, Rai, Reena, Mauck, Robert L., & Burdick, Jason A. (2013). The influence of hyaluronic acid hydrogel crosslinking density and macromolecular diffusivity on human MSC chondrogenesis and hypertrophy. *Biomaterials*, 34(2), 413-421. doi: <http://dx.doi.org/10.1016/j.biomaterials.2012.09.052>
- Billiet, Thomas, Vandenhaute, Mieke, Schelfhout, Jorg, Van Vlierberghe, Sandra, & Dubruel, Peter. (2012). Review: A review of trends and limitations in hydrogel-rapid prototyping for tissue engineering. *Biomaterials*, 33, 6020-6041. doi: 10.1016/j.biomaterials.2012.04.050
- Brownsey, Geoff J. (1993). Thermoreversible gelation of polymers and biopolymers. By Jean-Michel Guenet, Academic Press, London 1992, 278 pp., hardback £ 40, ISBN 0-12-305380-5. *Advanced Materials*, 5(3), 220-221. doi: 10.1002/adma.19930050316
- Bruyère, Olivier, Cooper, Cyrus, Arden, Nigel, Branco, Jaime, Brandi, Maria, Herrero-Beaumont, Gabriel, . . . Reginster, Jean-Yves. (2015). Can We Identify Patients with High Risk of Osteoarthritis Progression Who Will Respond to Treatment? A Focus on Epidemiology and Phenotype of Osteoarthritis. *Drugs & Aging*, 32(3), 179-187 179p. doi: 10.1007/s40266-015-0243-3
- Bryant, S. J., Bender, R. J., Durand, K. L., & Anseth, K. S. (2004). Encapsulating chondrocytes in degrading PEG hydrogels with high modulus: engineering gel structural changes to facilitate cartilaginous tissue production. *Biotechnol Bioeng*, 86(7), 747-755. doi: 10.1002/bit.20160
- Chang, Chunyu, Peng, Na, He, Meng, Teramoto, Yoshikuni, Nishio, Yoshiyuki, & Zhang, Lina. (2013). Fabrication and properties of chitin/hydroxyapatite hybrid hydrogels as scaffold nano-materials. *Carbohydrate Polymers*, 91(1), 7-13. doi: <http://dx.doi.org/10.1016/j.carbpol.2012.07.070>
- Chang, Nai-Jen, Jhung, Yi-Ru, Yao, Chih-Kai, & Yeh, Ming-Long. (2013). Hydrophilic gelatin and hyaluronic acid-treated PLGA scaffolds for cartilage tissue engineering. *Journal Of Applied Biomaterials & Functional Materials*, 11(1), e45-e52. doi: 10.5301/JABFM.2012.9253
- Chang, R., Nam, J., & Sun, W. (2008). Effects of dispensing pressure and nozzle diameter on cell survival from solid freeform fabrication-based direct cell writing. *Tissue Eng Part A*, 14(1), 41-48. doi: 10.1089/ten.a.2007.0004
- Chung, Cindy, & Burdick, Jason A. (2009). Influence of 3D Hyaluronic Acid Microenvironments on Mesenchymal Stem Cell Chondrogenesis. *Tissue Engineering. Part A*, 15(2), 243-254. doi: 10.1089/ten.tea.2008.0067
- Croisier, Florence, & Jérôme, Christine. (2013). Chitosan-based biomaterials for tissue engineering. *European Polymer Journal*, 49(4), 780-792. doi: <http://dx.doi.org/10.1016/j.eurpolymj.2012.12.009>

- Di Bella, Claudia, Fosang, Amanda, Donati, Davide M., Wallace, Gordon G., & Choong, Peter F. M. (2015). 3D Bioprinting of Cartilage for Orthopedic Surgeons: Reading between the Lines. *Frontiers in Surgery*, 2, 39. doi: 10.3389/fsurg.2015.00039
- Donaldson, James, Tudor, Francois, & McDermott, Ian D. (2015). (iv) Treatment options for articular cartilage damage in the knee. *Orthopaedics & Trauma*, 29(1), 24.
- El-Sherbiny, Ibrahim M., & Yacoub, Magdi H. (2013). Hydrogel scaffolds for tissue engineering: Progress and challenges. *Global Cardiology Science & Practice*, 2013(3), 316-342. doi: 10.5339/gcsp.2013.38
- Elisseeff, J., Anseth, K., Sims, D., McIntosh, W., Randolph, M., Yaremchuk, M., & Langer, R. (1999). Transdermal photopolymerization of poly(ethylene oxide)-based injectable hydrogels for tissue-engineered cartilage. *Plast Reconstr Surg*, 104(4), 1014-1022.
- Fathi, Ali, Lee, Sherry, Breen, Aishling, Shirazi, Ali Negahi, Valtchev, Peter, & Dehghani, Fariba. (2014). Enhancing the mechanical properties and physical stability of biomimetic polymer hydrogels for micro-patterning and tissue engineering applications. *European Polymer Journal*, 59, 161-170. doi: 10.1016/j.eurpolymj.2014.07.011
- Felimban, Raed, Ye, Ken, Traianedes, Kathy, Di Bella, Claudia, Crook, Jeremy, Wallace, Gordon G., . . . Myers, Damian E. (2014). Differentiation of Stem Cells from Human Infrapatellar Fat Pad: Characterization of Cells Undergoing Chondrogenesis. *Tissue Engineering: Part A*, 20, 2213.
- Flanigan, David, Harris, Joshua, Brockmeier, Peter, Lathrop, Rebecca, & Siston, Robert. (2014). The effects of defect size, orientation, and location on subchondral bone contact in oval-shaped experimental articular cartilage defects in a bovine knee model. *Knee Surgery, Sports Traumatology, Arthroscopy*, 22(1), 174-180.
- Hannoun, B. J., & Stephanopoulos, G. (1986). Diffusion coefficients of glucose and ethanol in cell-free and cell-occupied calcium alginate membranes. *Biotechnol Bioeng*, 28(6), 829-835. doi: 10.1002/bit.260280609
- Hao, T., Wen, N., Cao, J. K., Wang, H. B., Lu, S. H., Liu, T., . . . Wang, C. Y. (2010). The support of matrix accumulation and the promotion of sheep articular cartilage defects repair in vivo by chitosan hydrogels. *Osteoarthritis Cartilage*, 18(2), 257-265. doi: 10.1016/j.joca.2009.08.007
- Heino, J., Huhtala, M., Kapyla, J., & Johnson, M. S. (2009). Evolution of collagen-based adhesion systems. *Int J Biochem Cell Biol*, 41(2), 341-348. doi: 10.1016/j.biocel.2008.08.021
- Huang, Brian J., Hu, Jerry C., & Athanasiou, Kyriacos A. (2016). Review: Cell-based tissue engineering strategies used in the clinical repair of articular cartilage. *Biomaterials*, 98, 1-22. doi: 10.1016/j.biomaterials.2016.04.018
- Ju, Hee Kyung, Kim, So Yeon, & Lee, Young Moo. (2001). pH/temperature-responsive behaviors of semi-IPN and comb-type graft hydrogels composed of alginate and poly(N-isopropylacrylamide). *Polymer*, 42(16), 6851-6857. doi: [http://dx.doi.org/10.1016/S0032-3861\(01\)00143-4](http://dx.doi.org/10.1016/S0032-3861(01)00143-4)

- Karunanithi, Puvanan, Murali, Malliga Raman, Samuel, Shani, Raghavendran, Hanumanantha Rao Balaji, Abbas, Azlina Amir, & Kamarul, Tunku. (2016). Three dimensional alginate-fucoidan composite hydrogel augments the chondrogenic differentiation of mesenchymal stromal cells. *Carbohydrate Polymers*, 147, 294-303. doi: <http://dx.doi.org/10.1016/j.carbpol.2016.03.102>
- Kessler, Michael W., & Grande, Daniel A. (2008). Tissue engineering and cartilage. *Organogenesis*, 4(1), 28-32.
- Klotz, Barbara J., Gawlitta, Debby, Rosenberg, Antoine J. W. P., Malda, Jos, & Melchels, Ferry P. W. (2016). Gelatin-Methacryloyl Hydrogels: Towards Biofabrication-Based Tissue Repair. *Trends in Biotechnology*, 34(5), 394-407. doi: <http://dx.doi.org/10.1016/j.tibtech.2016.01.002>
- Kloxin, April M., Kasko, Andrea M., Salinas, Chelsea N., & Anseth, Kristi S. (2009). Photodegradable Hydrogels for Dynamic Tuning of Physical and Chemical Properties. *Science*, 324, 59-63.
- Kundu, J., Shim, J. H., Jang, J., Kim, S. W., & Cho, D. W. (2015). An additive manufacturing-based PCL-alginate-chondrocyte bioprinted scaffold for cartilage tissue engineering. *J Tissue Eng Regen Med*, 9(11), 1286-1297. doi: 10.1002/term.1682
- Levett, P. A., Melchels, F. P. W., Schrobback, K., Hutmacher, D. W., Malda, J., & Klein, T. J. (2014). A biomimetic extracellular matrix for cartilage tissue engineering centered on photocurable gelatin, hyaluronic acid and chondroitin sulfate. *Acta Biomaterialia*, 10(1), 214-223. doi: 10.1016/j.actbio.2013.10.005
- Levett, Peter A., Hutmacher, Dietmar W., Malda, Jos, & Klein, Travis J. (2014). Hyaluronic acid enhances the mechanical properties of tissue-engineered cartilage constructs. *PLoS ONE*, 9(12), e113216-e113216. doi: 10.1371/journal.pone.0113216
- Liao, E., Yaszemski, M., Krebsbach, P., & Hollister, S. (2007). Tissue-engineered cartilage constructs using composite hyaluronic acid/collagen I hydrogels and designed poly(propylene fumarate) scaffolds. *Tissue Eng*, 13(3), 537-550. doi: 10.1089/ten.2006.0117
- Lima, E. G., Bian, L., Mauck, R. L., Byers, B. A., Tuan, R. S., Ateshian, G. A., & Hung, C. T. (2006). The effect of applied compressive loading on tissue-engineered cartilage constructs cultured with TGF-beta3. *Conf Proc IEEE Eng Med Biol Soc*, 1, 779-782. doi: 10.1109/iembs.2006.259313
- Longworth, L. G. (1953). Diffusion Measurements, at 25°, of Aqueous Solutions of Amino Acids, Peptides and Sugars. *Journal of the American Chemical Society*, 75(22), 5705-5709. doi: 10.1021/ja01118a065
- Malda, Jos, Visser, Jetze, Melchels, Ferry P., Jüngst, Tomasz, Hennink, Wim E., Dhert, Wouter J. A., . . . Hutmacher, Dietmar W. (2013). 25th Anniversary Article: Engineering Hydrogels for Biofabrication. *Advanced Materials*, 25(36), 5011-5028. doi: 10.1002/adma.201302042
- Mandrycky, Christian, Wang, Zongjie, Kim, Keekyoung, & Kim, Deok-Ho. (2016). 3D bioprinting for engineering complex tissues. *Biotechnology Advances*, 34(4), 422-434. doi: <http://dx.doi.org/10.1016/j.biotechadv.2015.12.011>

- March, L. M., & Bagga, H. (2004). Epidemiology of osteoarthritis in Australia. *Med J Aust*, 180(5 Suppl), S6-10.
- Marchioli, G., van Gurp, L., van Krieken, P. P., Stamatialis, D., Engelse, M., van Blitterswijk, C. A., . . . van Apeldoorn, A. A. (2015). Fabrication of three-dimensional bioplotting hydrogel scaffolds for islets of Langerhans transplantation. *Biofabrication*, 7(2), 025009. doi: 10.1088/1758-5090/7/2/025009
- McKee, Clayton T., Last, Julie A., Russell, Paul, & Murphy, Christopher J. (2011). Indentation Versus Tensile Measurements of Young's Modulus for Soft Biological Tissues. *Tissue Engineering. Part B, Reviews*, 17(3), 155-164. doi: 10.1089/ten.teb.2010.0520
- Mondal, Shraddha, Haridas, Needa, Letha, S. Sneha, Vijith, V., Rajmohan, G., & Rosemary, M. J. (2016). Development of injectable high molecular weight hyaluronic acid hydrogels for cartilage regeneration. *Journal of Macromolecular Science: Pure & Applied Chemistry*, 53(8), 507-514. doi: 10.1080/10601325.2016.1189284
- Mueller, M. B., Fischer, M., Zellner, J., Berner, A., Dienstknecht, T., Prantl, L., . . . Angele, P. (2010). Hypertrophy in mesenchymal stem cell chondrogenesis: effect of TGF-beta isoforms and chondrogenic conditioning. *Cells Tissues Organs*, 192(3), 158-166. doi: 10.1159/000313399
- Murphy, Sean V., & Atala, Anthony. (2014). 3D bioprinting of tissues and organs. *Nat Biotech*, 32(8), 773-785. doi: 10.1038/nbt.2958
- Muzzarelli, Riccardo A. A., Greco, Francesco, Busilacchi, Alberto, Sollazzo, Vincenzo, & Gigante, Antonio. (2012). Review: Chitosan, hyaluronan and chondroitin sulfate in tissue engineering for cartilage regeneration: A review. *Carbohydrate Polymers*, 89, 723-739. doi: 10.1016/j.carbpol.2012.04.057
- Nair, Kalyani, Gandhi, Milind, Khalil, Saif, Yan, Karen Chang, Marcolongo, Michele, Barbee, Kenneth, & Sun, Wei. (2009). Characterization of cell viability during bioprinting processes. *Biotechnology Journal*, 4(8), 1168-1177. doi: 10.1002/biot.200900004
- Nichol, J. W., Koshy, S. T., Bae, H., Hwang, C. M., Yamanlar, S., & Khademhosseini, A. (2010). Cell-laden microengineered gelatin methacrylate hydrogels. *Biomaterials*, 31(21), 5536-5544. doi: 10.1016/j.biomaterials.2010.03.064
- O'Connell, D. Cathal, Claudia Di, Bella, Fletcher, Thompson, Cheryl, Augustine, Stephen, Beirne, Rhys, Cornock, . . . Gordon, G. Wallace. (2016). Development of the Biopen: a handheld device for surgical printing of adipose stem cells at a chondral wound site. *Biofabrication*, 8(1), 015019.
- Panadero, J. A., Lanceros-Mendez, S., & Ribelles, J. L. Gomez. (2016). Review article: Differentiation of mesenchymal stem cells for cartilage tissue engineering: Individual and synergetic effects of three-dimensional environment and mechanical loading. *Acta Biomaterialia*, 33, 1-12. doi: 10.1016/j.actbio.2016.01.037
- Paunipagar, Bhawan K., & Rasalkar, D. D. (2014). Imaging of articular cartilage. *The Indian Journal of Radiology & Imaging*, 24(3), 237-248. doi: 10.4103/0971-3026.137028

- Roughley, P. J., & Lee, E. R. (1994). Cartilage proteoglycans: structure and potential functions. *Microsc Res Tech*, 28(5), 385-397. doi: 10.1002/jemt.1070280505
- Roughley, P.J. (2006). The structure and function of cartilage proteoglycans. *PJ Roughley European Cells and Materials*, 12, 92-101.
- Ryan, Sarah. (2015). The challenge of managing osteoarthritis in primary care. *Practice Nurse*, 45(7), 36-40 35p.
- Saffarian, Mohammadreza, Mohammadi, Moona, & Mohammadi, Mohammadreza. (2015). Non-Newtonian Shear-Thinning Fluid Passing Through a Duct with an Obstacle, Using a Power Law Model. *Potenčni model pretoka nenewtonske tekočine s strižno odvisnim upadanjem viskoznosti skozi kanal z oviro.*, 61(10), 594-600. doi: 10.5545/sv-jme.2015.2650
- Selmi, T. A., Verdonk, P., Chambat, P., Dubrana, F., Potel, J. F., Barnouin, L., & Neyret, P. (2008). Autologous chondrocyte implantation in a novel alginate-agarose hydrogel: outcome at two years. *J Bone Joint Surg Br*, 90(5), 597-604. doi: 10.1302/0301-620x.90b5.20360
- Sharma, B., Williams, C. G., Khan, M., Manson, P., & Elisseeff, J. H. (2007). In vivo chondrogenesis of mesenchymal stem cells in a photopolymerized hydrogel. *Plast Reconstr Surg*, 119(1), 112-120. doi: 10.1097/01.prs.0000236896.22479.52
- Sivashanmugam, A., Arun Kumar, R., Vishnu Priya, M., Nair, Shantikumar V., & Jayakumar, R. (2015). An overview of injectable polymeric hydrogels for tissue engineering. *European Polymer Journal*, 72, 543-565. doi: <http://dx.doi.org/10.1016/j.eurpolymj.2015.05.014>
- Smith, C. M., Stone, A. L., Parkhill, R. L., Stewart, R. L., Simpkins, M. W., Kachurin, A. M., . . . Williams, S. K. (2004). Three-dimensional bioassembly tool for generating viable tissue-engineered constructs. *Tissue Eng*, 10(9-10), 1566-1576. doi: 10.1089/ten.2004.10.1566
- Sophia Fox, Alice J., Bedi, Asheesh, & Rodeo, Scott A. (2009). The Basic Science of Articular Cartilage: Structure, Composition, and Function. *Sports Health*, 1(6), 461-468. doi: 10.1177/1941738109350438
- Teixeira, J. A., Mota, M., & Venâncio, A. (1994). Model identification and diffusion coefficients determination of glucose and malic acid in calcium alginate membranes. *The Chemical Engineering Journal and the Biochemical Engineering Journal*, 56(1), B9-B14. doi: [http://dx.doi.org/10.1016/0923-0467\(94\)87026-8](http://dx.doi.org/10.1016/0923-0467(94)87026-8)
- Vandooren, J., Van den Steen, P. E., & Opdenakker, G. (2013). Biochemistry and molecular biology of gelatinase B or matrix metalloproteinase-9 (MMP-9): the next decade. *Crit Rev Biochem Mol Biol*, 48(3), 222-272. doi: 10.3109/10409238.2013.770819
- Visser, Jetze, Levett, Peter A., te Moller, Nikae C. R., Besems, Jeremy, Boere, Kristel W. M., van Rijen, Mattie H. P., . . . Malda, Jos. (2015). Crosslinkable Hydrogels Derived from Cartilage, Meniscus, and Tendon Tissue. *Tissue Engineering. Part A*, 21(7-8), 1195-1206. doi: 10.1089/ten.tea.2014.0362
- Woodfield, T. B., Malda, J., de Wijn, J., Peters, F., Riesle, J., & van Blitterswijk, C. A. (2004). Design of porous scaffolds for cartilage tissue engineering using a

- three-dimensional fiber-deposition technique. *Biomaterials*, 25(18), 4149-4161. doi: 10.1016/j.biomaterials.2003.10.056
- Xu, T., Jin, J., Gregory, C., Hickman, J. J., & Boland, T. (2005). Inkjet printing of viable mammalian cells. *Biomaterials*, 26(1), 93-99. doi: 10.1016/j.biomaterials.2004.04.011
- Xu, Tao, Kincaid, Helen, Atala, Anthony, & Yoo, James J. (2008). High-Throughput Production of Single-Cell Microparticles Using an Inkjet Printing Technology. *Journal of Manufacturing Science and Engineering*, 130(2), 021017-021017. doi: 10.1115/1.2903064
- Young, Simon, Wong, Mark, Tabata, Yasuhiko, & Mikos, Antonios G. (2005). Gelatin as a delivery vehicle for the controlled release of bioactive molecules. *Journal of Controlled Release*, 109(1-3), 256-274. doi: <http://dx.doi.org/10.1016/j.jconrel.2005.09.023>
- Yuan, Dechao, Chen, Zhu, Lin, Tao, Luo, Xuwei, Dong, Hua, & Feng, Gang. (2015). *Cartilage Tissue Engineering Using Combination of Chitosan Hydrogel and Mesenchymal Stem Cells* (Vol. 2015).